FINAL TECHNICAL REPORT
ON
MAGNETO-CHEMICAL CHARACTER STUDIES OF NOVEL Fe CATALYSTS FOR COAL LIQUEFACTION

Work Supported by

Department of Energy

Grant No. DE-FG22-96PC96225 (XU: 235-899)

Principal Investigator

Dr. Murty A. Akundi

Co-Investigators

Dr. Jian H. Zhang

Dr. A. N. Murty

Dr. S. V. Naidu

April 2002

FINAL TECHNICAL PROGRESS REPORT

Submitted to the U. S. Department of Energy

GRANT TITLE: **Magneto-Chemical Character Studies of Novel Fe Catalysts for Coal Liquefaction**

GRANT NO.: DE-FG22-96PC96225 (XU:235-899)

STARTING DATE: 01 October 1996

ENDING DATE: 30 September 2001

PROJECT DIRECTOR: MURTY A. AKUNDI
PHYSICS & DUAL DEGREE
ENGINEERING DEPARTMENT
Ph: 504-483-7647; Fax: 504-485-7911
e-mail: makundi@xula.edu

INSTITUTION: Xavier University of Louisiana
New Orleans, Louisiana 70125

*U.S./DOE Patent Clearance is not required prior to the publication of this document

_____
Project Director

_____
Date

TABLE OF CONTENTS

Introduction 1

Project Objective 3

Experimental: Instrumental

Mossbauer Studies 4

Zero Field NMR 5

Magnetic Measurements 7

FTIR 10

Worked Performed: Results and Discussion

Sample Preparation 14

I Effect of Metal loading

I.1 Fe/Mo Catalysts 16

I.1.1 FTIR Studies 16

I.1.2 Magnetization Studies 19

I.1.3 Catalytic Studies 23

I.2. Fe-Co-Mo Catalysts 24

I.2.1.1 FTIR Studies 24

1.2.2a Magnetization Studies 31

1.2.2b NMR Studies 32

1.2.3 Catalytic Studies 34

II Effect of Inter-metallic Ratio 40

FTIR Studies 40
III Effect of Method of preparation 47
FTIR Studies 47
IV Summary 56
References 57
Acknowledgements 61
Minority Undergraduate Student Training: Papers Presented 62

INTRODUCTION

Highly dispersed solid catalysts are very active in the conversion of coal to liquids[1]. Catalysts are widely used [2] to carry out several chemical reactions effectively, and are responsible for reduced production cost of many industrial products. More over the technology of catalysis is the heart of chemical and petroleum industries. Most of the **coal liquefaction catalysts** invariably contain ferromagnetic metals Fe/Co/Ni along with other transition elements, supports and promoters. Particle size, morphology, state of the unfilled d-shells and unpaired electrons and nature of the metallic charge distribution in the catalyst composite govern both the **catalytic** and **magnetic behavior** of the catalyst. Though much experimental data on catalytic yields are available, little effort has been devoted to correlating the physical and chemical characteristics of these inter-metallic clusters. Very little is understood about the specific roles of different elements in a catalyst. Many of the published results appear less selective and not easily reproducible[3]. Though much has been accomplished, considerable research is still needed to develop a firm scientific basis. The specific roles and functions of different elements in a catalyst composite, or how and why they influence the nature of the products are unclear. To gain a better understanding of the mechanisms involved, we have undertaken a detailed study of the **physico-chemica**l characteristics of both the chemisorbed molecules and the nano size catalyst particles.

Several important aspects related to characterization of syngas conversion catalysts and catalytic mechanisms have been studied [4]. Both surface and bulk techniques have been employed to understand their functionalities. Some techniques give information primarily about the chemisorbed molecules while others primarily about the changes in the surface layer of the adsorbent atoms. No single method can provide a total picture; a complete understanding will be possible when results from the several techniques are combined. Techniques such as Mossbauer spectroscopy, magnetization, X-ray diffraction, chemisorption, and Scanning Electron

Microscopy etc., provide valuable information concerning catalytic activity and selectivity as related to degree of reduction, degree of dispersion, method of impregnation, and influence of promoters.

Many questions regarding these catalysts need to be answered. Does an electronic interaction occur between the ferromagnetic metal (Fe/Co) and the support? Could such an interaction modify the electron density at the transition metal surface and lead to changes in the strength of the metal CO/H_2 bonds? How does a particular crystalline phase, such as hexagonal close packed (hcp) cobalt or face centered cubic(fcc) cobalt influence the catalytic character? How does a change in the intermetallic ratio alter the strength and character of CO, H_2 adsorption? The magnetic characterization techniques employed in this work, Mossbauer spectroscopy, Zero field Nuclear Magnetic resonance, and vibrational sample magnetometry are all sensitive to the crystalline phase and to changes in the electronic charge distribution around the transition metal nuclei. The FTIR studies provide information on the adsorbate gas molecule and the changes in the stretching frequencies of the adsorbate, reveal the nature of the gas metal interactions. The main focus of this study has been to examine the subtle changes that could occur in the catalytic and magnetic characters due to changes in composition and structure of the catalyst.

PROJECT OBJECTIVES:

The objectives of the present study are:

i) To synthesize iron catalysts: Fe/MoO_3, and $Fe/Co/MoO_3$ employing two distinct techniques: Pyrolysis with organic precursors and Co-precipitation of metal nitrates;

ii) To investigate the magnetic character of the catalysts before and after exposure to CO and $CO+H_2$ by a) Mossbauer study of Iron b) Zerofield Nuclear Magnetic Resonance study of Cobalt, and c) Magnetic character of the catalyst composite;

iii) To study the IR active surface species of the catalyst while stimulating (CO--Metal, $(CO+H_2)$--Metal) interactions, by FTIR Spectroscopy; and

iv) To anlyse the catalytic character (conversion efficiency and product distribution) in both direct and indirect liquefaction Process and

v) To examine the correlations between the magnetic and chemical characteristics

This report presents the results of our investigation on

a) the effect of metal loading b) the effect of intermetallic ratio and c) the effect of catalyst preparation procedure on i) the magnetic character of the catalyst composite ii) the IR active surface species of the catalyst and ii)the catalytic yields for three different metal loadings: 5%, 15%, and 25% (nominal) for three distinct intermetallic ratios (Fe/Co = 0.3, 1.5, 3.0)

EXPERIMENTAL: INSTRUMENTAL

A. **Mossbauer Studies (MB):**

The Mossbauer effect is the phenomenon of recoil-free fluorescence resonant absorption of gamma rays in solids. The phenomenon is very sensitive to the chemical bonding environment around nuclei (^{57}Fe) exhibiting this effect because the gamma ray energy is perturbed slightly. The three principal parameters obtained from a Mossbauer spectrum are the isomer shift (δ), the quadrupole splitting (ΔE_Q), and magnetic hyperfine splitting (H_n). The isomer shift originates from the interaction of electronic charge and nuclear charge, and is diagnostic of Fe oxidation state and spin state. The quadrupole splitting arises from an asymmetric charge distribution about ^{57}Fe nucleus which produces an electric field gradient (EFG) at the nucleus. The interaction of EFG with the nuclear quadrupole moment partially lifts the degeneracy of the nuclear energy levels, resulting in a quadrupole split spectrum. The quadrupole splitting provides information on the asymmetric nature of the ligands bonded to Fe and the non-spherical distribution of electrons over five 3d orbitals. The magnetic hyperfine splitting arises from the interaction of the nuclear magnetic dipole moment with a magnetic field, which lifts the remaining degeneracies of the nuclear energy levels. The magnetic hyperfine splitting leads to a variety of magneto-structural correlation based on the zero and/or high field Mossbauer spectrum of cooperatively ordered systems.

The advantage of Mossbauer spectroscopy lies in that it is not a bulk technique such as magnetization measurement, which is an average for all magnetic ions present. Mossbauer spectroscopy is specific to each individual metal ion site. In principal, this allows simultaneous measurements of all site magnetization in one zero field experiment. It is especially powerful when its application is correlated with the results of magnetization measurements. Fe based catalysts are ideally suited for study by Mossbauer spectroscopy to understand the role of iron in

catalytic reactions, as the composition of constituent metals changes. Mossbauer studies could reveal the correlation between catalytic activity and the nature of the solid state environment in the vicinity of Fe nucleus [5]. Distribution of particle size from iron oxide catalysts can be determined from the superparamgnetic Mossbauer spectra. We expect that Mossbauer studies along with the other diagnostic techniques employed, prove valuable in the design of efficient catalysts for coal liquefaction.

B. **Zero-field NMR Studies**: **(ZFNMR)**

Since its discovery by Gossard and Portis in 1959, nuclear magnetic resonance in ferromagnetic materials has provided information concerning hyperfine fields, and nuclear spin relaxation. Using this technique it is possible to characterize multi-domain, and superparamagnetic particles [6].

At the nuclei of atoms of ferro-, antiferro-, and ferrimagnetic materials there exists a strong internal magnetic field due to the partial polarization of s-electrons by the magnetic state of the material. This field, referred to as the hyperfine field, is the same field as described in Mossbauer spectroscopy. The interaction of the nuclear spin with the hyperfine field gives rise to a set of quantized energy states which lead to the well-known resonance condition $\omega = \gamma \mathbf{H_{hf}}$ where γ is the nuclear gyromagnetic ratio and $\mathbf{H_{hf}}$ is the hyperfine field. Thus, resonance conditions exist without the application of an external magnetic field, and through resonance techniques the internal field can be determined. It should be noted that the polarization of the s-electrons is a result of the electrostatic coupling of 3d (or 4f) electrons and s-electrons (both inner and outer s-band). As such the hyperfine field reflects the 3d electronic structure and behavior, and can provide valuable information if significant perturbations in the charge distribution occur due to syngas adsorption on the ferromagnetic metal or intermetallic interactions with in the metal cluster due to compositional changes or preparative techniques..

Adsorption of a molecule on the surface of ferromagnetic solid produces a change in the magnetization of the solid. If the adsorption process involves appreciable electronic interaction

and if the ratio of surface to volume in the adsorbent is large, then the fractional change of magnetization becomes substantial and lends itself to convenient measurement and interpretation [7]. The NMR line frequency can be represented by $\omega = \gamma (H_{hf} \pm \Delta H_{hf})$ where ΔH_{hf} represents the resulting modifications in the charge distribution in the vicinity of the cobalt nucleus due to the adsorbed molecule.

Figure 1 is a block diagram of the NQR/ZFNMR spectrometer system. The spectrometer is a conventional Superregenerative Oscillator (SRO) with Zeeman modulation and phase sensitive detection. It was designed by WILK's scientific corporation as a Nuclear Quadrupole Resonance spectrometer with a servo controlled self - quenching system for auto scan operation in the frequency range 2-350 MHz. Since Zeeman modulation is not suitable for ferromagnetic materials, frequency modulation was employed. This was easily accomplished using a woofer (low frequency) speaker to vibrate a small metal strip near the oscillator tank circuit.

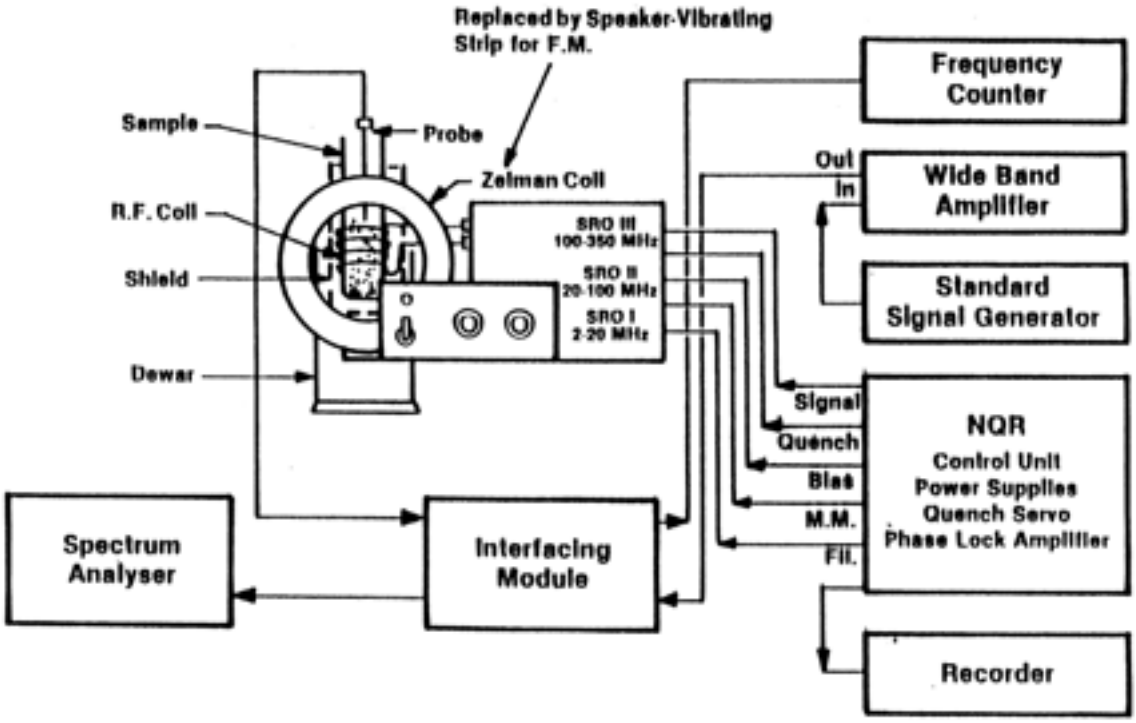

Figure 1 NMR/NQR SPECTROMETER SYSTEM BLOCK DIAGRAM.

The spectra were scanned in the 205-225 MHz region. The carrier frequency of the SRO was determined by displaying the oscillator output on a Tektronix 2712 spectrum analyzer. The scanning rate was 0.1MHz/min and the resonance frequencies were ascertained with an accuracy of ±0.3 MHz. A typical NMR spectrum of a catalyst sample is shown in Figure 2.

Figure 2: NMR Spectra of Fe-MoO3 Sample

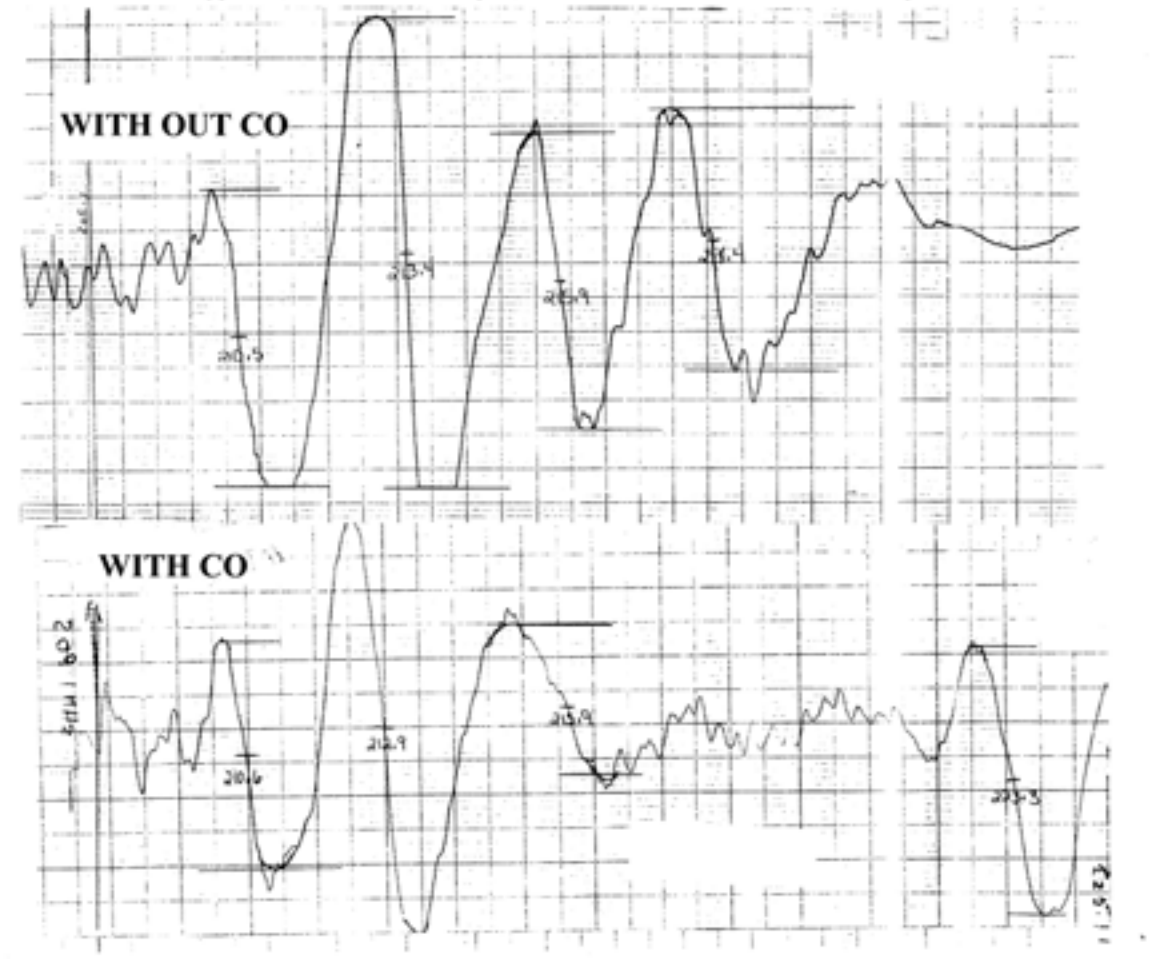

C. **Magnetic measurements**

Substances composed of atoms or ions with permanent magnetic moments arising from unpaired electron spins can be classified as para-, ferro-, antiferro-, or ferrimagnetic depending on such factors as exchange interaction between neighboring species, chemical composition, crystalline structure, crystal field effects, particle size, and temperature [8].

For paramagnetic behavior the magnetic susceptibility (χ) defined as the ratio of magnetization (M) to magnetic field (H), can be adequately described by the Curie Weiss law: $\chi = C/(T-\theta)$ where C and θ are the Curie and Weiss constants. When neighboring atoms or groups of atoms interact strongly and behave in a cooperative fashion, a ferromagnetic state exists with all spins 'parallel' in its domain.

Highly dispersed metals with metal crystallite sizes of less than single magnetic domain size exhibit unique magnetic properties [9]. Although the atoms which comprise these single domain particles are ferromagnetically coupled, the particles themselves behave like paramagnetic particles with very large magnetic moments. This gives rise to a behavior known as superparamagnetism. The magnetic moment associated with these superparamagnetic particles is directly proportional to the particle volume. The particle size can be determined from magnetization measurements [10]. Such analysis has been used to determine average particle size and particle size distribution for many highly dispersed metal catalysts [11-12]. Most heterogeneous catalysts are comprised of transition elements, their oxides or compounds, and often include various supports. The important characteristics of the transition elements are their incomplete d-electron shell and their unpaired electron spins. These features are responsible for their specific magnetic as well as their valuable catalytic properties.

Significant changes in the saturation magnetization M_s have been reported for a number of ferromagnetic catalysts due to chemisorption of H_2(H_2/Ni-Cu, H_2/Co, H_2/Fe). The change in magnetic moment per adsorbate atom/molecule, ε, in general can be represented by $\varepsilon = (\Delta M_0/M_0)\ n_{metal}\ \beta_{metal}/\ n_{gas}$. All the ferromagnetic metals were found to yield appreciable ε values: ε (Ni/H_2) = -0.37, ε (Co/H_2) = -0.54, ε (Fe/H_2) = +1.85. Very few studies have been made with CO as adsorbate. For adsorbates other than H_2 the magnetization studies yield ζ what is known as bond number $\zeta(x) = \varepsilon(x)/\ \varepsilon(H)$, where x is the adsorbate molecule. Thus the bond number indicates the number of adsorbent atoms involved in the interaction per adsorbate molecule, and one could postulate the possible nature of bonding.

The characteristic magnetic properties; M_S (saturation magnetization), M_r (remanent magnetization) and H_c (coercive field) have been determined using Digital Measurement Systems Vibrating Sample Magnetometer. Figure 3 is a block diagram of the experimental system. This is a Model 880A DMS VSM, with an accuracy of 1%, and a sensitivity of 50 micro EMU with one average. The sensitivity can be increased to 5 micro EMU with 100 averages. The system is microprocessor controlled and auto ranges full scale measurement from 0.04 EMU-4000 EMU. In the present arrangement a maximum magnetic field of 13.5 k.Oe can be applied and it can be programmed to make temperature dependent measurements in the range -192^{o}C to +740^{o}C. A typical hysteresis curve of a catalyst sample is shown in Figure 4.

FIGURE 3. DMS VIBRATING SAMPLE MAGNETOMETER

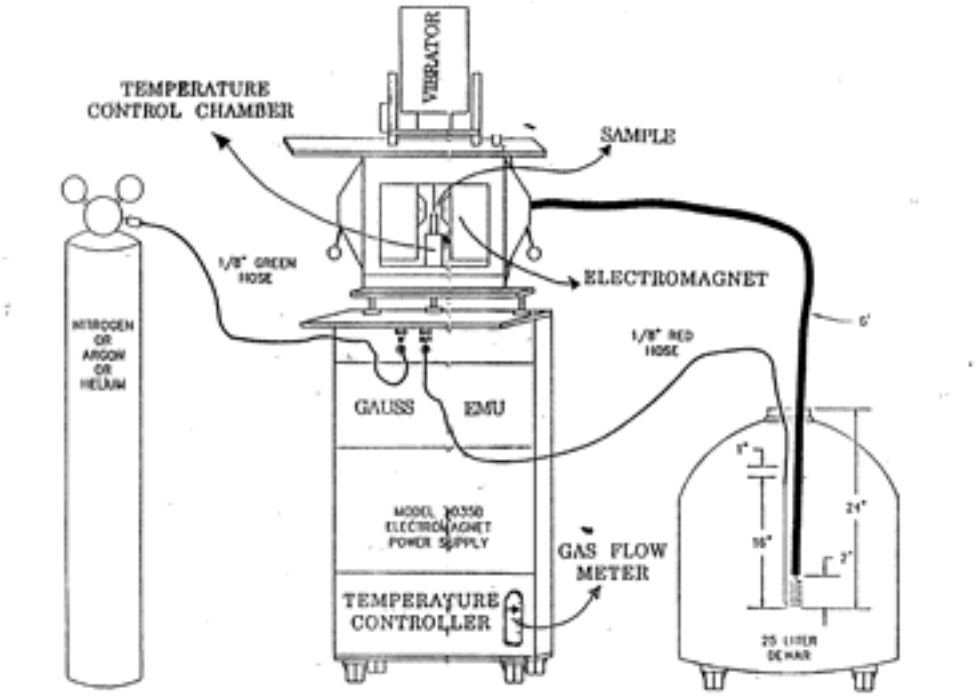

ZFNMR studies along with magnetic measurements have provided an excellent approach in our studies for the exploration of the magnetic nature of the inter-metallic interactions in the higher alcohol synthesis copper -cobalt catalyst systems [13-19].

FIGURE 4. HYSTERISIS CURVE OF A SAMPLE CATALYST

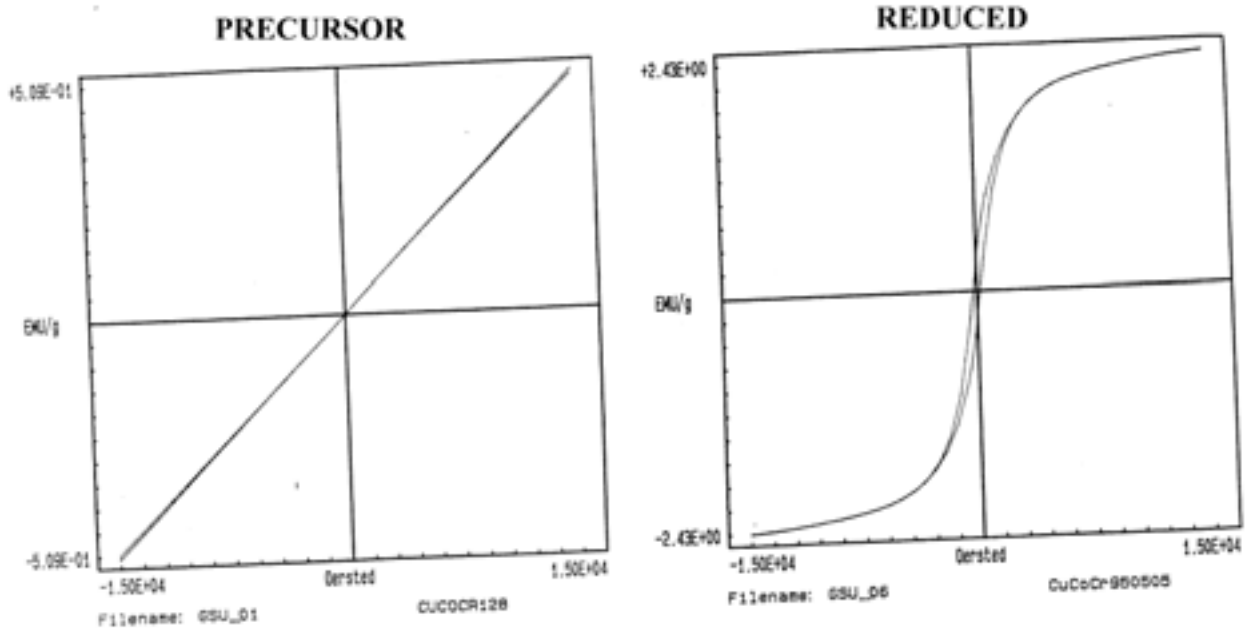

D. <u>Fourier Transform Infrared Spectroscopy (FTIR)</u>: Several investigators have successfully employed FTIR and IR spectroscopy techniques for the surface characterization of Cu/Co catalysts using CO as a probe molecule [20-24]. In general, spectroscopic techniques are found to be most precise in the analysis of vibrational and rotational structures of molecules [25, 26] When the probe molecule is adsorbed on the surface of the catalyst there are two possible electronic interactions between the adsorbent and the adsorbate. One is electron donation (s-electron) from the probe molecule to the empty d-orbital of the metal cation, the effect is strengthening of C-O bond of CO. Then ν shifts to higher frequency. The other interaction is the back- donation of the d-electron from the metal cation to an antibonding orbital of CO. The effect is weakening of the C-O bond of CO and ν_{CO} shifts to lower frequency. A knowledge of the change in the stretching frequency of CO reveals the nature and extent of intra and intermolecular interactions in the catalyst. The differences in the frequency shifts from one catalyst to the other which differ either in composition or preparative procedure would shed light on the catalytic character. The FTIR and magnetization studies complement each other in the

development of a picture of adsorbate and adsorbent interactions and their relation to observed selectivity character.

FTIR spectra of CO adsorbed Cu-Co catalysts were studied [24,25] using transmission spectroscopy. This technique seems to have several disadvantages. Most metal catalysts supported on metal oxides are opaque to IR radiation and the use of pressed discs, allows less surface area per gram of adsorbent available to adsorbate molecule. In recent years, Diffuse Reflectance Infrared Fourier Transform Spectroscopy (DRIFT) has been widely used [27-31] for powdered samples because of a) it's ease in sample handling, b) enhancement in percentage of absorption and c) increase in the area of contact of the adsorbent with the gas. In our FTIR studies, for investigation of CO adsorption frequencies we have employed DRIFT Technique.

The experimental set up consists of Mattison Research series FTIR spectrometer, equipped with an MCT detector operable in the mid IR region (4000-600cm^{-1}), a diffuse reflectance accessory, an environmental chamber and an automatic temperature controller.

A block diagram of the optics of the diffuse reflection attachment is shown in Figure 5. The praying mantis design incorporates two 6:1, 90^{o}off -axis ellipsoidal mirrors, M_3 and M_4, which subtend 20% of the 2 pi solid angle. These ellipsoids are arranged with a common focal point S. Mirrors M_1 and M_2 transfer the IR beam from the spectrometer to the first of these ellipsoids M_3. This ellipsoid focuses the beam onto the sample, S. The second ellipsoid (M_4) collects the radiation diffusely reflected from the sample. This radiation is then directed by mirrors M_5 and M_6 towards the detector. The environmental chamber (Figure 6), a stainless steel reaction chamber, consists of a sample cup to hold the sample, two windows at the entrance and exit positions for the incident and reflected infrared radiations. A third window is provided at the back of the chamber to illuminate or view the sample. In addition two entry ports are provided for evacuation and gas entry and another two for water circulation. The environmental chamber is also provided with an automatic temperature controller and can be heated up to

600ºC. Spectra can be recorded in the Mid-IR region at resolutions of 1, 2 or 4 cm^{-1}. The noise level can be decreased by increasing the gain and the number of scans.

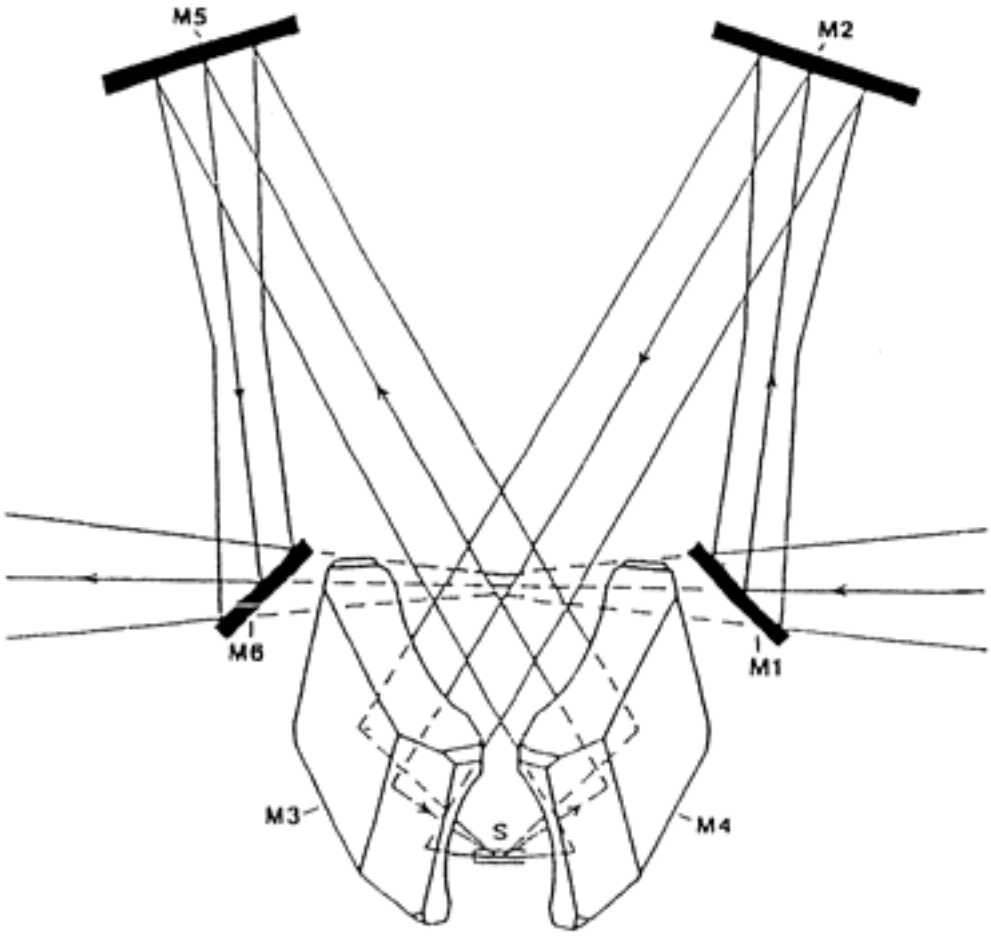

FIGURE 5: Block Diagram of the Optics of Diffused Reflection Attachment

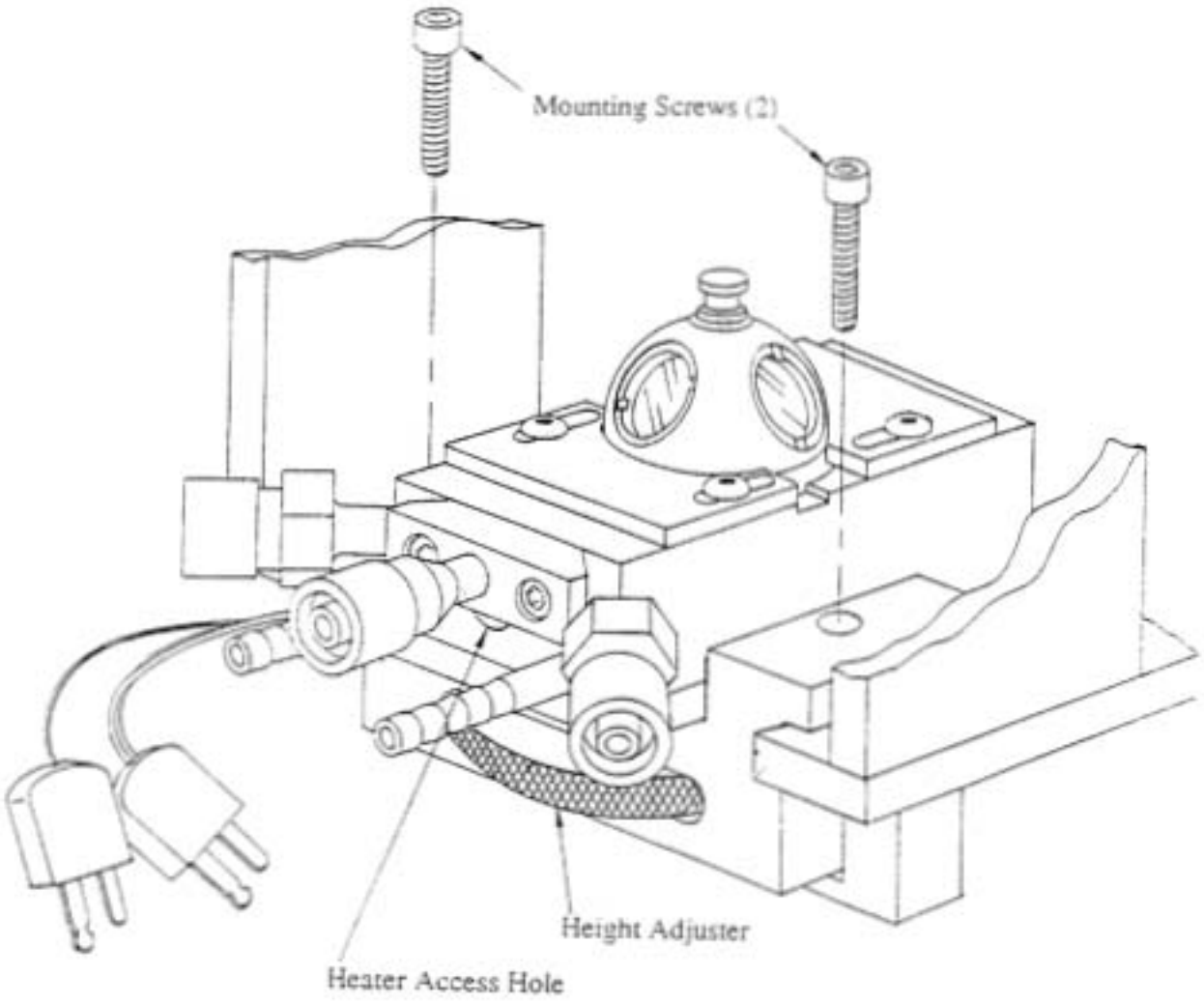

Figure 6. High Vacuum Environmental Chamber

WORK PERFORMED: RESULTS AND DISCUSSION

A: Sample preparation methods:

The surface composition and morphological character of the catalyst is sensitive to the method of preparation. Several research groups have developed synthetic procedures employing either co-precipitation or co-impregnation techniques[32-43] for preparation of catalysts. The control of conditions such as precipitation, pH and pre treatment (drying, calcination, and reduction) seems to be critical for the activity of the catalyst prepared. Apart from these conventional procedures, aerogel [44,45] and pyrolysis techniques [46] seem to produce highly dispersed metal oxides or oxide solutions. The small particles produced with high surface area and porosity by these techniques are ideal for catalysis. Fine particles are also known to exhibit a unique magnetic property called "Superparamagnetism". The few studies that have been made using such specialized catalysts indicate that their activity and selectivity is about two to three orders of magnitude higher than conventional catalysts [47,48].

a) *Co-Precipitation method*:

A total of twelve samples were prepared using co-precipitation method. Three samples contained iron and molybdenum with Fe/MoO_3 ratios of 5%, 15%, and 25% respectively. Nine samples contained Iron, cobalt and molybdenum with Fe/CO of 0.3, 1.5, 3.0 and Fe/Co/MoO_3 at a metal loading of 5%, 15%, and 25% respectively. In a typical preparation a 0.2 M metal nitrate solution or solution mixture was added to 0.1 M molybdate solution made from ammonium para molybdate at a rate of 3.5 – 4.0 ml/min vii burette while stirring. The pH of the solution was 5.6-5.7 at the beginning of the precipitation process. After completion of the precipitation, the mixture was kept stirring for 1 hr and standing for 24 hrs. The resulting gelatin was stirred again adding 50 ml of water, filtered, and rinsed. The precipitate was dried at 70°C in a vacuum oven

over night and ground to a fine powder for calcination. The sample was calcined at 400ºC for 18 hrs. These precursors were used for Mossbauer FTIR, NMR, and Magnetization studies.

b) *Pyrolysis method*;

The organic precursor method was used for preparation of homogeneous and highly dispersed multiphase oxides. The synthesis started with preparation of a solution that contained all required cations and citric acid, and followed by a rapid dehydration to form an organic precursor citrate. Pyrolysis of the precursor at a low temperature resulted in the formation of the fine particles of the mixed oxides. The same metal loading and intermetallic ratios used for the twelve co-precipitation sample studies were repeated for samples prepared by pyrolysis technique.

In a typical preparation, solid MoO_3 was dissolved in aqueous solution with adding ammonia drop-wise and then mixed with iron (III) and cobalt (II) nitrate solutions. Citric acid solution was added to the solution at a ratio of one mole of citric acid to one mole of metal ion. The solution was heated at 70-80ºC on a hot plate while stirring for rapid dehydration. The dehydrated gel precursor was dried over night at 80ºC in an oven. The dried precursor was smashed and ground to a fine powder in mortar and then combusted in an oven for one hour. The percent yields for all samples were higher than 95%.

For Mossbauer, NMR and magnetization studies, the samples were reduced in a glass tube for 18 hrs at 400ºC in a flowing stream of hydrogen. The sample tube is sealed under partial pressure of argon and was sent to Grambling State University for magnetization studies. Carbon monoxide or CO + H_2 was adsorbed on the reduced samples for 2 hrs at 250ºC and the samples tubes were sealed under partial vacuum. These were used for syn-gas interaction studies.

The following procedure was adopted for all samples to obtain the FTIR spectra of the precursor, reduced, CO adsorbed and syngas ($CO+H_2$) adsorbed samples. To obtain the spectra of the precursor, first a background spectrum of KBr was taken at a scan rate of 500, resolution of 4 cm^{-1} and a gain of 4. Then each catalyst was mixed with KBr and loaded into the sample cup of the Drift accessory and evacuated for two hours at 80ºC to remove moisture and any adsorbed gases. IR spectra were recorded for each sample at 50ºC, 100ºC and 200ºC. Maintaining the same scan rate and resolution. The background spectrum was subtracted from the ample spectrum and the resulting spectrum was analyzed. To obtain FTIR spectra of the reduced sample, the precursor spectrum was used as background and the sample was reduced in a flowing stream of hydrogen for 18 hrs at 400ºC. Spectra were taken 50ºC, 100ºC, and 200ºC. To obtain the carbon monoxide and syngas ($CO+H_2$) adsorbed spectra the following procedure was employed. The samples were reduced at 400ºC under continuous hydrogen flow at a rate of 20 cc/min. After reducing the sample for 18 hrs, hydrogen was out gassed and the temperature was decreased to room temperature. A background scan of the reduced sample was taken. CO was admitted at room temperature, and while continuing the CO flow, FTIR spectra were recorded as the temperature was increased in increments of 50ºC till 250ºC. Then CO was disorbed and FTIR spectra were taken in the reverse order. The same procedure was employed for syngas adsorbed samples.

I. Effect of Metal Loading:

I.1 Fe/Mo Catalysts:

I.1.1: FTIR studies

a) *Co-Precipitation catalysts:*

Three catalysts with Fe/Mo ratios of 5%, 15% and 25% were prepared using co-precipitation of nitrates. Vibrational frequencies of the IR active species along with the possible

assignments are presented in Table 1A. Using FTIR and magnetization techniques, the catalyst behavior was examined for four different phases. i) as prepared (precursor) ii) after reduction by passing hydrogen (reduced) iii) after exposure to CO and iv) finally exposing to $CO+H_2$ (syngas).

Earlier investigators [49,50] on precursors have attributed bands in the region 600 – 1000 cm^{-1}, to Mo-O, Mo = O, Fe – O – Mo vibrations. The additional bands we observed in the region 1600 – 2000 cm^{-1} have not been reported earlier in the literature. We believe these bands could be due to Fe – MoO_3 vibrations, similar to mono-dentate and bi-dentate ligand structures of metal carbonates as suggested by Davydov[51].

There seems to be no significant differences in the vibrational modes due to changes in percent metal loading. However in the precursor and reduced samples, the higher vibrational modes (1900-2900 cm^{-1}) remain persistent at lower metal loading of 5%. Exposure to CO or $CO+H_2$ seems to suppress these high frequency modes irrespective of the amount of iron content in catalyst composite. These findings suggest that, exposure to syngas seems to dissociate the MoO_3 ligand structures without generating carbonyls of iron. In these catalysts it is likely that iron carbides might be forming instead of carbonyl, which are essential intermediate products for the formation of longer chain hydrocarbons.

TABLE 1A: Fe-MoO_3 Co-Precipitation Catalysts Effect of metal loading

Precursor			Reduced			+CO			+($CO+H_2$)			Assignments
25%	15%	5%	25%	15%	5%	25%	15%	5%	25%	15%	5%	
2929		2927										Fe-MoO_3
		2852										Fe-MoO_3
1928	1949	1952			1937							Fe-MoO_3
					1901							Fe-MoO_3
		1887	1848	1846	1837							Fe-MoO_3
1753	1769	1742	1712	1699	1692							Fe-MoO_3
1612	1615	1615										Fe-MoO_3
				1504	1514							Fe-MoO_3
		1455	1488									Fe-MoO_3
			1261	1265								Fe-MoO_3
1150			1147									Fe-MoO_3
						1039	1044				1054	MoO_3
994	994	989		1002	998		989	986	996			Mo=O
958	957		933			974		958	971	967	961	Fe-O-Mo
					918			917	934	924		Fe-O-Mo
862	842	875	857			884		871	882	874		Mo-O
				832	832	831			838	835	831	Mo-O
787							791	814	813	813	762	Mo-O
									780	767		Mo-O
				731						737		Mo-O
		697						688			695	Fe-O

b) Pyrolysis catalysts:

FTIR data on pyrolysis samples is presented in Table 1B. Samples prepared by the pyrolysis technique also do not show any changes in the surface species as metal loading changes. That means the additional iron loaded into the composite does not alter any possible surface interactions with the incoming gases. Again exposure to CO and $CO+H_2$ seems to suppress the high frequency vibrational modes due to Fe-MoO_3 structures. These findings suggest that ferric molybdate may not be a suitable catalyst for syngas conversion.

TABLE 1B: Effect of metal Loading: Fe-MoO_3 (Pyrolysis Samples)

Precursor			Reduced			+CO			+($CO+H_2$)			Assignments
25%	15%	5%	25%	15%	5%	25%	15%	5%	25%	15%	5%	
	1949	1954										Fe-MoO_3
1901	1924											Fe-MoO_3
		1884	1863	1849					1845			Fe-MoO_3
1760	1752	1759										Fe-MoO_3
			1702	1672	1682	1687	1711		1665			Fe-MoO_3
1610												Fe-MoO_3
			1509						1536			Fe-MoO_3
1410												Fe-MoO_3
1329			1323									Fe-MoO_3
						1281						Fe-MoO_3
						1240		1236				Fe-MoO_3
1150	1123	1124			1106	1116	1106	1105				Fe-MoO_3
		1026		1003	1004		1010	1015		1015	1017	MoO_3
958	957	961				982	979		975	981		Mo-O
908	903	905			932	937	936	937		943		Mo-O
				861			844	842		883	847	Mo-O
787	791	798	812							761		Fe-O
			718									Fe-O
											697	Fe-O

I.1.2: Magnetization studies:

Iron Molybdenum catalysts with three different metal loadings (Fe/Mo =5% and Fe/Mo =15% and Fe/Mo = 25%) were examined. Their magnetic and Mossbauer characteristics were determined as: i) Precursor (as prepared) ii) reduced (passing hydrogen over the sample for 18 hours at 400°C) iii) after exposing the sample to carbon monoxide and syngas. The experimental results were presented in Tables 2 and 3.

As iron content increases there appears a consistent increase in the paramagnetic nature of the composite. However the excess loaded iron is not amenable for reduction or surface

interaction with the incoming gases CO or $CO+H_2$. Comparison of the data of pure samples (Table2A-CRC handbook) with the catalysts we prepared clearly shows that the susceptibility of MoO_3 drastically drops with the addition of iron. It seems that iron and MoO_3 form a complex resulting in filling of the d-orbitals of both iron and MoO_3. (Fe: $3d^6 4s^2$, Mo: $4d^5 5s^1$) The unpaired spins seem to be quenched in the ligand formations. Increase in metal loading though leads to a slight increase in the susceptibility value of the whole composite, the ferromagenic component σ – emu per gram of the loaded metal decreases. This indicates that increase in Fe metal loading leads to an increase in ligand formations with MoO_3 resulting in a decrease of unpaired electrons in the Fe-MoO_3 structures. From the data Table 2B, it seems the structure of the composite changes as metal loading changes. At higher metal loading iron molybdate could be forming which is not amenable for reduction.

Mossbauer results are presented in Table 3. The absence of Quadrupole splitting ΔE in the Mossbauer spectra of the precursors indicates that the electron configuaration of iron is (Fe^{3+}) $3d^5$ and that Fe is in a $6s_{1/2}$ ionic state. The half filled 3d shell forms a spherically symmetric charge distribution and does not therefore contribute to the electric filed gradient (q) Both $q_{valence}$ and q_{ionic} are zero. There exist no ionic charges in the precursor of the Fe-Mo composite. It is reported that [52] Fe^{3+} in oxidic matrices shows chemical shifts (isomeric shift) in the range 0.47- 0.6 mm/s. The observed shift in the Fe-Mo composites studied is about 0.68, indicating that the precursor, as expected, is in a Fe-MoO_3 matrix. When exposed to carbon monoxide, substantial quadrupole splitting occurs (ΔE = 0.79 and 0.75 mm/s) indicating appreciable ionic charge production occurs in the lattice. In addition CO adsorption leads to the production of Fe^{2+} species with an outer electron configuration $3d^{6-x}\ 4s^x$, x ~ 10% as per the Walker, Werthiem Jaccarino graph [15]. Almost identical situation is observed for both 5% and 15% iron samples. Adding hydrogen along with CO increases the quadrupole splitting in the 15% samples and decreases in the 5% sample. This means lattice ion concentration is promoted

by increasing the iron content in the composite. Syngas adsorption also generates Fe^{2+} species but with almost no 4s population approaching a complete $3d^6$ configuration. Both CO and $CO+H_2$ addition seem to result in charge transfer to the metal atom as well as to the lattice.

TABLE 2A: χ Values of Pure Compounds

Sample	χ (emu/g.Oe)
Pure FeO	0.09
Pure (Fe_2O_3)	0.11
Pure(MoO_3)	$90x10^{-6}$
Pure Mo	$837X10^{-6}$
MoO_2	$81`0x10^{-6}$
Mo_3O_8	42 cgs
Mo_2O_3	Diamagnetic - 42 cgs
O_2	3449 cgs
O_2	3449 cgs

TABLE 2B

			χ (10^{-6} emu/g.Oe)		
	Sample	%Fe	Precipitated	Calcined	Reduced
1	$Fe_2(MoO_4)_3$	26	27	37	33
2	$Fe_2O_3.12MoO_3$	6.5	14.2	19.6	13.8

TABLE 2C: Fe-MoO_3 Co-Precipitation Catalysts: Effect of Metal Loading

Fe-MoO_3 Co-Precipitation catalysts : Effect of Metal Loading								
	Precursor		**Reduced**		**+ CO**		**+($CO+H_2$)**	
ML	χ(10^{-6} emu/g.Oe)	σ (emu/gM)	χ(10^{-6} emu/g.Oe)	σ (emu/gM)	χ(10^{-6} emu/g.Oe)	σ (emu/gM)	χ(10^{-6}emu/g.Oe)	σ (emu/gM)
5%	14		13	10.4	12	1.4	11	0.26
15%	27		16	0.66	17	0.33	13	0.13
25%	31		20	0.12	21	0.24	21	0.08

TABLE 3: Mossabauer Results: Effect of Metal Loading

	Precursor			**Reduced**			**+CO**			**+(CO+H2)**		
ML	Oxidation state	Chemical shift (mm/s)	Quadrupole Splitting (mm/s)	Oxidation state	Chemical shift (mm/s)	Quadrupole Splitting (mm/s)	Oxidation state	Chemical shift (mm/s)	Quadrupole Splitting (mm/s)	Oxidation state	Chemical shift	Quadrupole Splitting (mm/s)
5%	Fe^{3+}	0.670		Fe^{3+}	0.590		Fe^{3+} Fe^{2+}	0.685 1.160	0.790 1.740	Fe^{3+} Fe^{2+}	0.720 1.295	0.660 1.810
15%	Fe^{3+}	0.680		Fe^{3+} Fe^{2+}	0.684 1.125	0.828 1.710	Fe^{3+} Fe^{2}	0.685 1.160	0.750 1.700	Fe^{3+} Fe^{2+}	0.740 1.220	0.820 1.780

I 1.3 Catalytic Studies: Indirect Liquefaction

Two samples with metal loading of 25%, 15%, were sieved to 60/100 mesh. Then a 1.0 gram sample was loaded and reduced in the reactor using 4% H_2 in He. The exact protocol employed with these samples was similar to the previous studies [54] with Cu-Co-Cr samples. Each catalyst was then tested for catalytic activity at 280ºC and 900 psi total pressure with an inlet gas composition of $H_2/CO/N_2$ equal to 40/40/20. Nitrogen was the internal standard for calculation of carbon mass balances. Each catalyst was tested for 2 days at steady state. Total time on line with catalyst reduction was 4 days. The catalytic yields are given in tables 4A and 4B. The results show mainly low chain hydrocarbon products, with the highest yield for methane. These results support our FTIR and Magnetization findings and suggest that Fe-Moly catalysts are good oxidative dehydrogenation catalysts and poor syngas conversion catalysts. In direct liquefaction studies with both pyrolysis and co-precipitation samples we did not observe any bond-clevage of the model compound naphthyl bibenzylmethane.

TABLE 4A

Sample	CO conversion (%)	Product			
		Total hydrocarbon (%)	CO_2 (%)	CH_3OH (%)	Unknown (%)
Fe/Mo (25%)	3.5	54.2	22.7	2.0	20.6
Fe/Mo (15%)	0.4	61.2	23.1	1.7	15.0

TABLE 4B

Sample	Product				
	Methane	Ethane	Ethylene	Propane	Butane
Fe/Mo (25%)	38.8	8.3	0.8	5.1	1.2
Fe/Mo (15%)	42.9	9.4	0.7	5.8	1.4

I.2 Fe-Co-MoO_3 Catalysts

Three catalysts were prepared with increasing Fe/Co ratios (0.3, 1.5, and 3.0) using co-precipitation and pyrolysis methods. Each catalyst was reacted with ammonium para molybdate to yield three different loadings 25%, 15%, and 5%. Using FTIR and Magnetization techniques the catalyst behavior is examined for the four phases of treatment: precursor, reduced, exposure to CO and finally exposure to syngas. Catalytic studies were performed using direct liquefaction method.

1.2.1 FTIR studies:

a) *Co-Precipitation catalysts:*

Tables 5-7 presents the vibrational frequencies along with suggested assignments for three different inter-metallic ratios at different metal loadings. At each metal ratio for the three different metal loadings, we observed bands due to Fe-MoO_3, Fe-O, Fe-O-Mo and Mo-O vibrations which were also found in Fe-Mo catalysts. In addition we observed additional vibrational frequencies due to cobalt IR active surface species. At higher metal loadings (25% and 15%), we observe more vibrational modes due to mono-dentate and bi-dentate structures of Fe/Co with MoO_3 in all four phases of the catalyst.. However as cobalt content increases, even at 5% metal loading, mono-dentate and bi-dentate structures of Fe-MoO_3 and Co-MoO_3 seem to be forming. This means that that cobalt is more active in forming ligand with MoO_3 than iron. Another feature that has been observed at all metal loadings is the absence of MoO_3 bulk phase vibrations near 1000 cm^{-1}, in the precursor but distinctly prominent in reduced, CO and Syngas adsorbed samples. Syngas and CO exposure seems to promote reduction of the metal oxide and detach MoO_3 ligands from metal oxides and enhance MoO_3 vibrations. Also we observed

decrease in the number of vibrational modes due to surface IR active Fe -MoO_3 and Co-MoO_3 vibrations confirming the earlier observations with Iron–Moly catalysts.

TABLE 5: Effect of Metal Loading: Fe-Co-MoO_3 (Co-Precipitation samples) Fe/Co =0.3

Precursor			Reduced			+CO			+($CO+H_2$)			Assignment
25%	15%	5%	25%	15%	5%	25%	15%	5%	25%	15%	5%	
1951		1950								1939	1940	Fe-MoO_3
1922	1923	1922	1939									Co-MoO_3
			1902	1901	1903							Fe-MoO_3
1881	1879	1880										Fe-MoO_3
			1838	1811								Co-MoO_3
1754			1784	1724		1723			1720	1717		Fe-MoO_3
			1683	1687		1656			1663	1664		Co-MoO_3
1613	1615	1621				1623						Fe-MoO_3
				1583		1581	1583			1584		Co-MoO_3
1509			1532	1524					1509		1510	Fe-MoO_3
				1486		1480	1486	1456		1478		Fe-MoO_3
1407	1408					1416	1420		1419	1450		Co-CO_3
			1386	1385	1386							Co-MoO_3
1334				1326					1337	1301		Fe/Co-MoO_3
						1268	1269			1268	1251	Co-CO_3
						1218				1234		Co-CO_3
1161						1167						Fe-MoO_3
1133	1127	1141									1146	Fe-MoO_3
				1102	1104	1118	1112	1101	1113	1109	1102	Fe/Co-MoO_3
						1048	1035		1040	1060	1052	MoO_3 BP*
			1006	1007	1005	1006	1007	1015	1006	1006	1001	MoO_3 BP*
993	991	994										Mo=O
957	963					973	978					Fe-O
			940	940	930	933	932	937	951	927	927	Mo-O
882		874										Mo-O
838	832	832				836			835			Mo-O
												Mo-O
782					799		801			807	808	Mo-O
	731	749						752				Mo-O
686						684			689	681		Fe-O

*BP=Bulk Phase

TABLE 6: Effect of Metal Loading: Fe-Co-MoO_3 (Co-Precipitation samples) Fe/Co =1.5

Precursor			Reduced			+CO			+($CO+H_2$)			Assignment
25%	**15%**	**5%**	**25%**	**15%**	**5%**	**25%**	**15%**	**5%**	**25%**	**15%**	**5%**	
1938	1936	1939								1945		Fe-MoO_3
				1901	1903		1910			1910		Fe-MoO_3
			1853	1841			1856		1850	1856		Co-MoO_3
1764									1741			Fe-MoO_3
	1727			1705						1690		Co-MoO_3
			1675			1662	1678		1651			Co-MoO_3
1612	1608	1621				1627						Fe-MoO_3
						1589						Co-MoO_3
				1511			1515			1529	1520	Fe-MoO_3
			1482			1461		1460	1466	1493		Fe-MoO_3
1416	1427					1415			1430	1443		Co-MoO_3
				1395								Co-MoO_3
										1327		Co-CO_3
						1276	1270				1267	Co-CO_3
									1150			Fe-MoO_3
1115	1127	1121		1115	1112	1105	1102	1102	1104	1105	1105	Fe/Co-MoO_3
			1002	1005	1007	1005	1005	1008	1006	1005	1006	MoO_3 BP*
	993	994										Mo=O
961			960			969	967		971	968		Fe-O
			940	939	942	931		937	923	936	930	Mo-O
895			895									Mo-O
	820	825		822								Mo-O

*BP=Bulk Phase

TABLE 7: Effect of Metal Loading: Fe-Co-MoO_3 (Co-Precipitation samples) Fe/Co =3.0

Precursor			Reduced			+CO			+($CO+H_2$)			Assignment
25%	**15%**	**5%**	**25%**	**15%**	**5%**	**25%**	**15%**	**5%**	**25%**	**15%**	**5%**	
1924	1942											Co-MoO_3
				1903	1902							Fe-MoO_3
	1881	1883										Fe-MoO_3
			1851	1840		1858	1864	1854	1854	1861		Co-MoO_3
1738								1740		1715		
			1695	1692	1683	1682	1693					Co-MoO_3
1615	1615	1614						1624	1645			Fe-MoO_3
			1515	1518		1500	1512	1502	1521	1517		Fe-MoO_3
1417	1415	1413										Co-MoO_3
			1385	1394		1384		1354			1389	Co-MoO_3
			1289		1269	1289				1266	1273	Co-CO_3
							1232					Co-CO_3
1148												Fe-MoO_3
	1119	1124									1106	Fe/Co-MoO_3
									1048		1039	MoO_3 BP*
							1019	1025		1018		MoO_3 BP*
		985			997							Mo=O
	971		968			968	977	962	977			Fe-O
				954						939	942	Mo-O
896								842	826			Mo-O
	791											Mo-O
		748								735	733	Mo-O
									691		693	Fe-O
					673		673				676	Fe-O

*BP=Bulk Phase

b) *Pyrolysis samples*:

Tables 8 to 10 present the data on the samples made by pyrolysis technique. In these samples, increasing the metal loading from 5% to 25% shows no significant changes in the vibrational spectra of the surface species. This feature seems to be common for all the three inter-metallic ratios.

TABLE 8: Effect of metal loading pyrolysis samples: Fe/Co (0.3)

Precursor		Reduced		+CO		+(CO+H_2)		Assignment
15%	**5%**	**15%**	**5%**	**15%**	**5%**	**15%**	**5%**	
1954	1956	1941	1932		1946	1947	1945	Fe-MoO_3
1920	1919	1905	1903	1928		1903	1908	Fe/Co-MoO_3
1886	1888			1866	1859	1859	1844	Fe-MoO_3
				1808	1802		1776	Co-MoO_3
	1732	1730	1722	1733	1738		1706	Fe-MoO_3
	1662			1667	1657	1680	1647	Co-MoO_3
1615	1598			1623	1605			Fe-MoO_3
			1558	1576		1573		Co-MoO_3
	1533				1533		1530	Fe-MoO_3
	1481	1495		1491	1472	1504		Fe-MoO_3
1410	1417				1415			Co-MoO_3
	1374		1393					Co-MoO_3
				1334	1357	1342	1343	$CoCO_3$
					1250		1290	$CoCO_3$
						1208	1228	$CoCO_3$
1127	1128						1156	Fe-MoO_3
			1108		1107	1105	1105	Fe-MoO_3
1071	1067					1046	1063	MoO_3 BP*
		1009	1008	1036	1024		1016	MoO_3 BP*
937		946		960		951		Fe-O
	921		927		916		920	Mo-O
				889	870	884	869	Mo-O
863	849	851	845					Mo-O
		771	762	744	758	754	756	Mo-O
709	719					704		Fe-O

*BP=Bulk Phase

TABLE 9: Effect of metal loading pyrolysis samples: Fe/Co (1.5)

Precursor			Reduced			+CO			+(CO+H_2)			**Assignment**
25%	15%	5%	25%	15%	5%	25%	15%	5%	25%	15%	5%	
	1952	1955			1942					1940	1946	Fe-MoO_3
1919	1919			1901				1927	1913		1909	Co-MoO_3
	1883	1885										Fe-MoO_3
			1852	1841		1851			1843	1860	1866	Fe-MoO_3
						1800			1778			Co-MoO_3
1761	1748			1748	1736					1725		Fe-MoO_3
				1710		1713	1714	1713				Fe-MoO_3
			1695						1685	1666		Co-MoO_3
1615	1608											Fe-MoO_3
			1542	1545	1567	1562	1540	1523	1540	1557	1568	Fe-MoO_3
1505			1499			1488				1483		Fe-MoO_3
				1423	1441				1450			Co-MoO_3
1406								1401		1404		Co-MoO_3
			1385			1388	1376		1372			Co-MoO_3
1307									1306	1329		Co-MoO_3
			1296			1271				1275		Co-MoO_3
						1237						Co-MoO_3
									1160	1178	1152	Co-CO_3
1144	1129	1129										Fe-MoO_3
			1119		1118	1099		1116		1109	1104	Fe/Co-MoO_3
		1076				1077					1052	MoO_3 BP*
								1026	1032		1017	MoO_3 BP*
			989	998		982	1000					Mo=O
952		958							972			Fe-O
					937	929		936		938	941	Mo-O
	903		909									Mo-O
887									890			Mo-O
					862			863		863	844	Mo-O
	817	819	831			825			826			Mo-O
				784			781					Mo-O
			753			764		759			765	Mo-O
712						712	706					Fe-O

*BP=Bulk Phase

TABLE 10: Effect of metal loading pyrolysis samples: Fe/Co (3.0)

Sample			Reduced			+CO			+(CO+H_2)			**Assignment**
25%	15%	5%	25%	15%	5%	25%	15%	5%	25%	15%	5%	
		1956			1932			1946		1946	1945	Fe-MoO_3
1928	1921	1924	1900	1901	1903	1906	1909	1908	1905		1909	Co-MoO_3
1886	1882	1887					1866	1864		1864		Fe-MoO_3
			1852	1840		1840	1825		1846			Co-MoO_3
1748	1749	1771				1780		1791	1782	1793	1775	Fe-MoO_3
		1721			1707	1715	1731		1730	1717		Co-MoO_3
			1697	1693		1688	1680	1687	1693		1679	Co-MoO_3
		1663				1653				1652		Co-MoO_3
1612	1611	1596					1600		1620		1607	Fe-MoO_3
	1566			1540	1548			1570	1550	1540	1564	Co-MoO_3
	1502		1511			1525	1499		1511		1515	Fe-MoO_3
		1476						1476	1462		1484	Co-MoO_3
		1434						1440			1430	Co-MoO_3
1417	1411		1396		1392			1400		1400	1400	Co-MoO_3
				1356		1377	1388		1369			Co-MoO_3
	1327						1325	1300		1320	1300	Co-MoO_3
			1280						1280	1264		Co-MoO_3
							1227	1226			1228	Co-CoO_3
						1200				1190		Co-CoO_3
							1159	1153		1152	1156	Co-CoO_3
	1123	1127			1107			1104	1104		1105	Fe/Co-MoO_3
		1075				1075		1062	1061	1050	1061	MoO_3 BP*
	1030						1035	1020			1017	MoO_3 BP*
			992	995	1005							Mo=O
967	956	963		960		975	977	978	975		977	Mo-O
			947		936	921	938	938	935		940	Mo-O
	901	898		897				875				Mo-O
882	865				870		843	853		843	868	Mo-O

*BP=Bulk Phase

1.2.2a Magnetization studies:

The result of magnetization studies are presented in Tables 11-13. The following conclusion were made from the magnetization studies.

1. All the catalysts show very poor magnetic behavior as compared to the innate strong ferromagnetic character of metal ingredients. (σ_{Fe} = 218 emu/g, σ_{Co} = 161 emu/g)
2. The metals seem to form complexes with molybdena and remain not amenable for reduction as shown by the very low saturation magnetization (σ) and susceptibility (χ) values for all samples as compared to the values for ferromagnetic metals.
3. There seem to be no significant changes in the magnetic character of the composite due to interaction between CO/CO+H_2 and the composite.
4. Iron seems to interact strongly with the support than cobalt and remains irreducible as indicated by higher sigma values as Fe/Co ratio decreases.
5. At higher metal loading more complexation of the metals with molybdena seems to occur as indicated by the lower σ values at 25% metal loading compared to the 15% and 5% metal loading. This effect is more evident as Fe/Co ratio decreases.
6. The paramagnetic nature of the composite decrease as the metal loading decreases.

TABLE 11: Fe- Co-MoO_3 Co-Precipitation catalysts(Fe/Co =0.3): Effect of Metal Loading

ML	Precursor		Reduced		+ CO		+(CO+H_2)	
	$\chi(10^{-6}$ emu/g.Oe)	σ (emu/gM)	$\chi(10^{-6}$ emu/g.Oe)	σ (emu/gM)	$\chi(10^{-6}$ emu/g.Oe)	σ (emu/gM)	$\chi(10^{-6}$ emu/g.Oe)	σ (emu/gM)
5%	3.4		3.3	0.32	3	0.2	3.6	0.1
15%	1.2		2.3	0.21	2.1	0.2	2.3	0.46
25%	17		1.3	0.19	1.2	0.12	0.96	0.09
Fe/Co =1.5								
5%	2.8		9.6	0.44	9.3	0.6	9.3	0.84
15%	17.8		11.8	0.27	17	0.4	11.5	0.13
25%	25		31.6	3.36	41.7		19.5	

TABLE12: Fe-Co-MoO_3-Pyrolysis Samples: Effect of metal Loading

		FE/CO (3.0)			FE/CO (1.5)			FE/CO (0.3)		
		RED	CO	$CO+H_2$	RED	CO	$CO+H_2$	RED	CO	$CO+H_2$
25%	σ (emu/gM)	0.63	0.27	0.57	0.29	0.23	0.18	0.93	0.92	0.7
	χ (10^{-6} emu/g.Oe)	34.9	36.5	26	34.7	36	40	32.6	33.5	37.7
		RED	CO	$CO+H_2$	RED	CO	$CO+H_2$	RED	CO	$CO+H_2$
15%	σ (emu/gM)	0.98	0.33	2.67	2	1.7	1.73	14.5	12.8	31.9
	χ (10^{-6} emu/g.Oe)	22	19.5	21.5	23.9	22.8	20	22.8	23.9	25
		RED	CO	$CO+H_2$	RED	CO	$CO+H_2$	RED	CO	$CO+H_2$
5%	σ (emu/gM)	0.2	0.6	0.25	0	1.9	5.7	4.4	21	22
	χ (10^{-6} emu/g.Oe)	11	11	4.6	11	8.8	7.9	8.4	9	8.7

1.2.2b NMR studies:

NMR frequencies of the catalysts studied are presented in Table 13. None of the samples exhibit the normal cobalt lines. Most of the lines observed are above the HCP line frequency indicating that cobalt is alloyed with other metals in the composite. In general we find when the cobalt content is high (Fe/Co = 0.3) some cobalt HCP phase particles occur. As iron content increases (Fe/Co=1.5) we find only alloyed Co lines indicating that there occurs inter-metallic interaction between Co and Fe. It appears no significant changes occur in the NMR spectrum due to exposure to CO or syngas or increasing metal loading. That means cobalt remains inactive, interlocked in the lattice with MoO_3 ligands or Fe.

TABLE 13: NMR DATA: Fe-CO-MoO_3 Co-Precipitation Catalysts : Effect of Inter meatallic ratio/ metal loading

ML 5%								
Precursor		**Reduced**		**+CO**		**+(CO+H2)**		
Fe/C0 (0.3)	Fe/CO (1.5)	Fe/CO (0.30)	Fe/CO (1.5)	Fe/CO (0.30)	Fe/CO (1.5)	Fe/CO (0.30)	Fe/CO (1.5)	
219								Co Fault line
221		221		221				Co HCP line
222	222				222	222		Alloyed Co line
		223	223	223	223		223	Alloyed Co line
224	224			224	224	224	224	Alloyed Co line
225								Alloyed Co line
		226						Alloyed Co line
ML 15%								
							221	Co HCP line
	222	222		222		222		Alloyed Co line
223					223		223	Alloyed Co line
	224	224	224	224	224	224		Alloyed Co line
225								Alloyed Co line
ML 25%								
221		221	221					Co HCP line
222	222	222		222		222		Alloyed Co line
			223		223		223	Alloyed Co line
224	224	224	224	224		224	224	Alloyed Co line
					225			Alloyed Co line

I 2.3 Catalytic Studies:

Catalytic studies: Direct Liquefaction:

Table 14A and B present the catalytic yields at different metal loadings. The synthesized iron, cobalt, and molybdenum based catalysts using both co-precipitation method and pyrolysis method were evaluated for selective C-C bond scission using the model compound, naphthyl bibenzylmethane (NBBM), and hydrogen donating solvent, 9,10–dihydrophenanthrene. Naphthyl bibenzylmethane (NBBM) has been used extensively as a model compound for studying catalytic activity towards bond scission reaction relevant to coal liquefaction due to the presence of both monocyclic and bicyclic aromatic units as well as the various types of cleavable C-C bonds. The structure of naphthyl bibenzylmethane with possible sites of bond breakages and the products due to varieties of C-C bond scission are shown in Figure 1.

The model compound catalyst tests were carried out at 400^{o}C using the standard procedure developed in DOE laboratory [55]. A Pyrex tube of about 5 mL volume was loaded with 25 mg of naphthyl bibenzylmethane, 100 mg of 9,10 –dihydrophenanthrene, 10 mg of element sulfur, and 10 mg catalyst powder, and sealed under vacuum. In the first run, thirteen Pyrex tubes were loaded into a Parr stainless steel bomb reactor: one tube containing no catalyst as a reference, three tubes containing iron and molybdenum based materials, and nine tubes containing iron, cobalt, and molybdenum based materials prepared by co-precipitation method. In the second run, all materials were prepared using the pyrolysis method. After that, about 5 mL tetrahydronaphthalene was added in the bomb as a heat transfer medium and pressure counterbalance. A thermocouple directly measured the temperature inside the bomb. A typical heat-up time was 40 min to 400^{o}C, and 60 min kept at 400^{o}C. Then the power was turned off, and the bomb was naturally cooled down. After the bomb was open, all Pyrex reaction tubes

were cleaned with methylene chloride. The tubes were opened at room temperature after immersed in ice water for cooling down. The content of each tube was extracted with 2.0 mL of HPLC grade methylene chloride containing a fixed concentration (1000 ppm) of tert-butylbenzene, which was used as an internal standard. The clear aliquots were kept in tightly closed vials.

The aliquots were analyzed on a HP5890 GC/MASS. The GC temperature program consisted of a 10^{o}C/min ramp from 40 to 150^{o} C, followed by a 30^{o}C/min ramp, where the temperature was held for 30 min until the model compound eluted.

The GC/MASS spectrum for the reference sample without the catalyst is shown in Figure 2. Under the measurement condition, the retention times are 6.0 min for the internal standard, tert-butylbenzene; 14.2 min and 14.7 min for 9,10-dihydrophenanthrene, and its product, phenanthrene, after dehydrogenation at high temperature, respectively, and 21.5 min for NBBM product. The GC/MASS result of the reference sample indicates that no bond breakage occurs in the model compound without catalyst under the experiment condition. The GC/MASS spectra for all six samples, which contain iron oxide and molybdenum oxide but no cobalt oxide, show basically the same features as observed for the reference sample, indicating ferric molybdate and molybdenum oxide do not have catalytic activity on the model compound. However, all samples containing cobalt oxide exhibit four additional peaks in their GC/MASS spectra. They represent the compounds formed due to bond breakages in site ***a*** and ***b*** in the model compound, and are listed as follows with retention times: naphthalene (9.30 min), methylbibenzyl (13.7 min), methylnaphthalene (11.1 min), and bibenzyl (13.1 min). A typical GC/MASS spectrum for is shown in Figure 3. The relative abundance of these products deducted from GC spectra is

summarized in Tables 14A and 14B with all values relative to the internal standard. It is observed that the samples with composition of $2.0Fe_2(MoO_4)_3$:$1.2CoMoO_4$:MoO_3 prepared by both co-precipitation and citrate precursor methods have the lowest activity. We are unable to explain the observation at this moment. Naphthalene and methylbibenzyl are the products due to the breakage of bond ***a***, whereas methylnaphthalene and bibenzyl are products due to breakage of bond ***b***. The abundances of naphthalene and methylbibenzyl for the samples prepared by both methods is approximately three time as large as those of methylnaphthalene and bibenzyl, indicating that the breakage of bond ***a*** is more favorable. That is because that the breakage of bond ***a*** would produce a highly stable compound, naphthalene.

FIGURE 1. Structure and major reaction products of naphthylbibenzylmethane

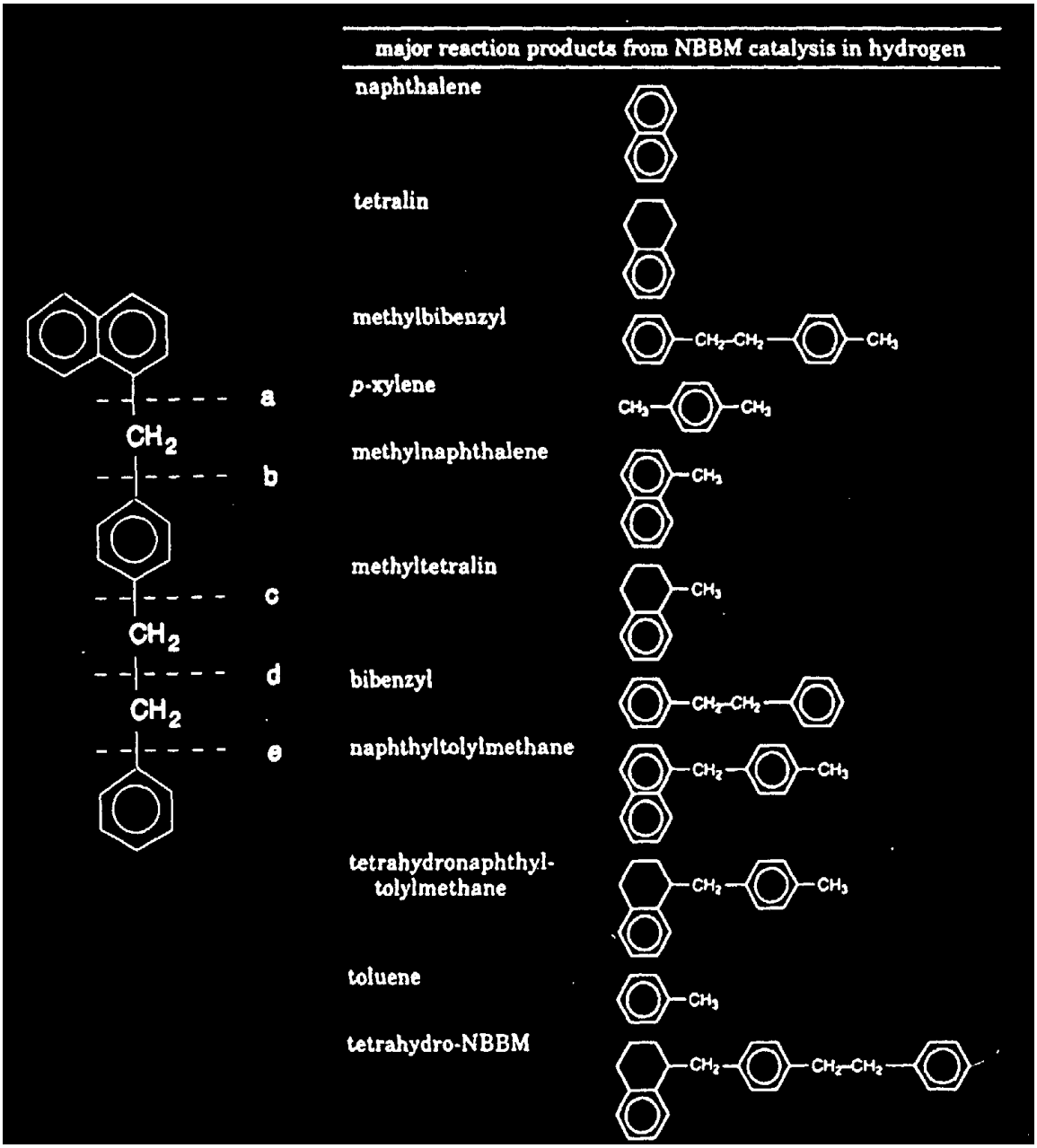

FIGURE 2. GC spectrum of the sample with no catalyst

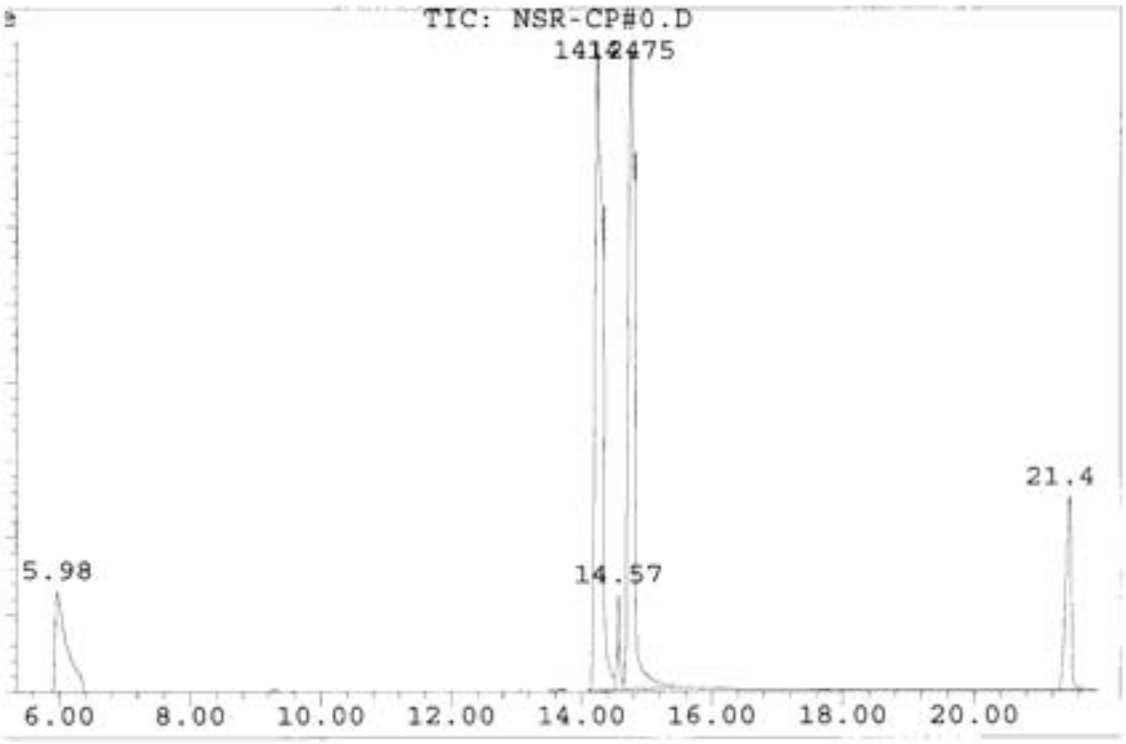

FIGURE 3. GC spectrum of the sample with FeCo/MoO2=5% and Fe/Co=3.0

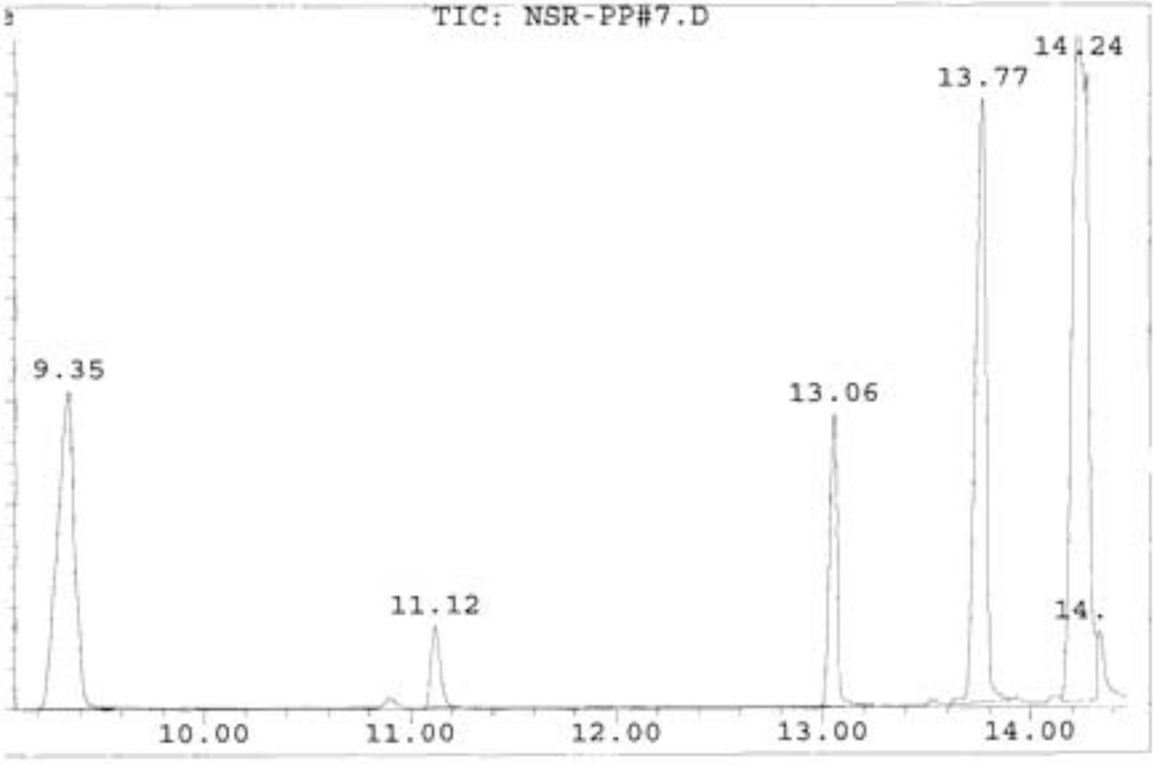

TABLE 14A Effect of Metal Loading – Co-Precipitation Catalysts

Product	Fe/Co =3.0			Fe/Co =1.5			Fe/Co =0.3	
	25%	15%	5%	25%	15%	25%	15%	5%
Naphthalene	0.623	3.76	3.26	3.06	3.42	3.13	3.36	2.42
Mythyl Bi-benzyl	0.644	4.43	3.84	2.95	3.98	3.1	3.74	2.94
Methyl Naphthalene	0.070	0.564	0.452	0.424	0.515	0.508	0.529	0.356
Bi-benzyl	0.265	1.60	1.33	1.57	1.60	1.33	1.32	0.709

TABLE 14B Effect of Metal Loading – Pyrolysis Catalysts

Product	Fe/Co =3.0			Fe/Co =1.5			Fe/Co =0.3	
	25%	15%	5%	25%	15%	5%	15%	5%
Naphthalene	3.0	1.34	1.80	1.77	2.19	2.07	2.35	2.03
Mythyl Bi-benzyl	0.662	1.90	1. 98	1.59	1.71	1.85	1.79	1.76
Methyl Naphthalene	0.626	0.35	0.267	0.198	0.344	0.277	0.323	0.303
Bi-benzyl	0.069	0.874	0.550	0.934	0.867	0.62	0.842	0.653

II. Effect of Inter-metallic ratio

FTIR Studies

a) *Co-Precipitation samples*:

Vibrational frequencies of the samples (Fe/Co = 0.3, 1.5, and 3.0) were compared at different metal loadings. The data of the observed frequencies is presented in tables 15-17. It seems when iron content is high (Fe/Co =3.0) more IR active surface structures occur in all the reduced, CO or syngas exposed samples. Low frequency vibrational modes seem more prominent at higher cobalt concentration. As metal loading increases more IR active surface Co-MoO_3 ligand structures seem to be forming. While both Fe and Co atoms increase in the lattice at higher metal loading, there appears more vibrational modes in the samples with inter-metallic ratio Fe/Co =0.3. This means that on the surface there occur more Co-MoO_3 ligands than Fe-MoO_3 ligands.

b) *Pyrolysis samples*:

From the data presented in Tables 18-20, one strong feature that emerges is that in pyrolysis samples more IR active surface species seems to be present compared to coprecipitation samples. In general at Fe/Co = 1.5, there seems to occur fewer IR active surface species vibrations. Both higher iron and cobalt (Fe/Co = 3.0, Fe/Co = 0.3) samples show active surface vibrations. This indicates at the mid ratio (Fe/Co = 1.5) Fe and Co may be forming alloy clusters inhibiting interactions with MoO_3.

As indicated in Table 11, σ value increases as Fe/Co ratio decreases. It suggests that iron seems to interact strongly with the support than cobalt. From the NMR table, when cobalt content is high some cobalt phase particles occur. As cobalt content decreases we find only alloyed cobalt lines indicating that there occurs an inter-metallic interaction between Co and Fe.

It seems that the catalytic reactivity is relatively consistent in both series independent of $FeCo/MoO_3$, and Fe/Co ratios.

TABLE 15: Effect of Inter-metallic ratio: Fe-Co-MoO_3 (Co-Precipitation Samples) ML 5%

Precursor			Reduced			+CO			+($CO+H_2$)			Assignment
3.0	1.5	0.3	3.0	1.5	0.3	3.0	1.5	0.3	3.0	1.5	0.3	
	1939	1950									1940	Fe-MoO_3
		1922	1902	1903	1903							Fe/Co-MoO_3
1883		1880										Fe-MoO_3
						1854						Co-MoO_3
						1740						Fe-MoO_3
			1683									Co-MoO_3
1614	1621	1621				1624						Fe-MoO_3
						1502				1520	1510	Fe-MoO_3
							1460	1456				Fe-MoO_3
1413												Co-CO_3
					1386	1354			1389			Co- MoO_3/CO_3
			1269						1273	1267	1251	Co-CO_3
1124	1121	1142									1146	Fe-MoO_3
				1112	1104		1102	1101	1106	1105	1102	Fe/Co-MoO_3
						1025			1039			MoO_3 BP*
				1007	1005		1008	1015		1006	1001	MoO_3 BP*
985	994	994	997			962						Mo=O
				942	930		937	937	942	930	927	Mo-O
		874										Mo-O
	825	832				842						Mo-O
					799						808	Mo-O
748		749						752	733			Mo-O
									693			Fe-O
			673						676			Fe-O

*BP=Bulk Phase

TABLE 16: Effect of Inter-metallic Ratio: Fe-Co-MoO_3 (Co-Precipitation Samples) ML 15%

Precursor			Reduced			+CO			+($CO+H_2$)			Assignments
3.0	1.5	0.3	3.0	1.5	0.3	3.0	1.5	0.3	3.0	1.5	0.3	
1942	1936	1923								1945	1939	Fe/Co-MoO_3
			1903	1901	1901		1910			1910		Fe-MoO_3
1881		1879				1864	1856		1861	1850		Fe-MoO_3
			1840	1841	1811							Co-MoO_3
	1727			1705	1724				1715	1741	1717	Fe-MoO_3
			1692		1687	1693	1678			1651	1664	Co-MoO_3
1615	1608	1615										Fe-MoO_3
					1583			1583			1584	Co-MoO_3
			1518	1511	1524	1512	1515		1517			Fe-MoO_3
					1486			1486		1466	1478	Fe-MoO_3
1415	1427	1408						1420		1430	1450	Co-CO_3
			1394	1395	1385							Co-MoO_3
					1326						1301	Fe/Co-MoO_3
							1270	1269	1266		1268	Co-CO_3
						1232					1234	Co-CO_3
	1127	1127										Fe-MoO_3
1119				1115	1102		1102	1112		1104	1109	Fe/Co-MoO_3
								1035			1060	MoO_3 BP*
				1005	1007	1019	1005	1007	1018	1006	1006	MoO_3 BP*
971	993	991				977	967	978		971		Mo=O
		963	954	939	940			932	939	923	927	Mo-O
791	820	832		822				801			807	Mo-O
		731							735			Fe-O
						673					681	Fe-O

*BP=Bulk Phase

TABLE 17: Effect of Inter-metallic Ratio: Fe-Co-MoO_3 (Co-Precipitation Samples) ML 25%

Precursor			Reduced			+CO			+($CO+H_2$)			Assignments
3.0	1.5	0.3	3.0	1.5	0.3	3.0	1.5	0.3	3.0	1.5	0.3	
		1951										Fe-MoO_3
1924	1938	1922			1939							Co-MoO_3
		1881			1902							Fe-MoO_3
			1851	1853	1838	1858			1854	1850		Co-MoO_3
	1764	1754			1784							Fe-MoO_3
1738								1723		1741	1720	Fe-MoO_3
			1695	1675	1683	1682	1662	1656	1645	1651	1663	Co-MoO_3
1615	1612	1613						1623				Fe-MoO_3
							1589	1581				Co-MoO_3
		1509	1515		1532	1500			1521		1509	Fe-MoO_3
				1482			1461	1480		1466		Fe-MoO_3
1417	1416	1407					1415	1416		1430	1419	Co-MoO_3
			1385		1386	1384						Fe/Co-MoO_3
		1334									1337	
						1289	1276	1268				Co-CO_3
								1218				Co-CO_3
1148		1161						1167		1150		Fe/Co-MoO_3
	1115	1133					1105	1118		1104	1113	Fe/Co-MoO_3
								1048	1048		1040	MoO_3 BP*
				1002	1006		1005	1006		1006	1006	MoO_3 BP*
		993										Mo=O
	961	957	968	960		968	969	973	977	971		Mo-O
				940	940		931	933		923	927	Mo-O
896	895	882		895								Mo-O
		836						836	826		807	Mo-O
		782										Mo-O
		686						684	691		681	Fe-O

*BP=Bulk Phase

TABLE 18: Effect of Inter-metallic Ratio: Fe-Co-MoO_3 (Pyrolysis samples) ML=5%

Precursor			Reduced			+CO			+($CO+H_2$)			Assignment
3.0	**1.5**	**0.3**	**3.0**	**1.5**	**0.3**	**3.0**	**1.5**	**0.3**	**3.0**	**1.5**	**0.3**	
1956	1955	1956	1932	1942	1932	1946		1946	1945	1946	1945	Fe-MoO_3
1924		1919	1903		1903	1908	1927		1909	1909	1908	Fe/Co-MoO_3
1887	1885	1888				1864		1859		1866	1844	Fe-MoO_3
1771						1791		1802	1775		1776	Fe-MoO_3
1721		1732	1707	1736	1722		1713	1738			1706	Co-MoO_3
						1687			1679			Fe-MoO_3
1663		1662						1657			1647	Co-MoO_3
1596		1598						1605	1607			Fe/Co-MoO_3
				1567	1558	1570			1564	1568		Co-MoO_3
		1533	1548				1523	1533	1515		1530	Co-MoO_3
1476		1481				1476		1472	1484			Fe-MoO_3
1434				1441		1440			1430			Fe-MoO_3
		1417				1400	1401	1415	1400			Co-CO_3
		1374	1392		1393							
								1357			1343	Co-CO_3
						1300			1300		1290	Co-CO_3
						1226		1250	1228		1228	Co-CO_3
						1153			1156	1152	1156	Co-CO_3
1127	1129	1128	1107	1118	1108	1104	1116	1107	1105	1104	1105	Fe/Co-MoO_3
1075	1076	1067				1062			1061	1052	1063	MoO_3 BP*
						1020	1026	1024	1017	1017	1016	MoO_3 BP*
			1005		1008							MoO_3 BP*
963	958					978			977			Mo=O
		921	936	937	927	938	936	916	940	941	920	Mo-O
898						875						Mo-O
		849	870	862	845	853	863	870	868	844	869	Mo-O
825	819											Mo-O
					762	764	759	758	762	765	756	Mo-O
709		719	725									Fe-O

*BP=Bulk Phase

TABLE 19: Effect of Inter-metallic Ratio: Fe-Co-MoO_3 (Pyrolysis samples) ML=15%

Precursor			Reduced			+CO			+($CO+H_2$)			Assignment
3.0	**1.5**	**0.3**	**3.0**	**1.5**	**0.3**	**3.0**	**1.5**	**0.3**	**3.0**	**1.5**	**0.3**	
	1952	1954			1941				1946	1940	1947	Fe-MoO_3
1921	1919	1920	1901	1901	1905	1909		1928			1903	Co-MoO_3
1882	1883	1886										Fe-MoO_3
			1840	1841		1866		1866	1864	1860	1859	Fe-MoO_3
						1825		1808	1793			Fe-MoO_3
1749	1748			1748								Fe-MoO_3
				1710	1730	1731	1714	1733	1717	1725		Fe-MoO_3
			1693			1680		1667	1652	1666	1680	Co-MoO_3
1611	1608	1615				1600		1623				Fe-MoO_3
1566			1540	1545			1540	1576	1540	1557	1573	Co-MoO_3
1502					1495	1499		1491		1483	1504	Fe-MoO_3
1411		1410		1423					1400	1404		Co-MoO_3
			1356			1388	1376					Co-MoO_3
1327						1325		1334	1320	1329	1342	Co-CO_3
									1264	1275		Co-CO_3
						1227			1190		1208	Co-CO_3
						1159			1152	1178		Co-CO_3
1123	1129	1127										Fe-MoO_3
										1109	1105	Co-CO_3
		1071							1050		1046	MoO_3 BP*
1030						1035		1036				MoO_3 BP*
			995	998	1009		1000					Mo=O
			960			977		960				Mo-O
956		937			946	938				938	951	Mo-O
901	903		897					889			884	Mo-O
865		863			851	843			843	863		Mo-O
	817		816								805	Mo-O
793				784	771		781					Mo-O
						757		744			754	Mo-O
		709					706		708		704	Fe-O

*BP=Bulk Phase

TABLE 20: Effect of Inter-metallic Ratio: Fe-Co-MoO_3 (Pyrolysis samples) ML=25%

Precursor		Reduced		+CO		+($CO+H_2$)		Assignment
3.0	**1.5**	**3.0**	**1.5**	**3.0**	**1.5**	**3.0**	**1.5**	
1928	1919						1913	Co-MoO_3
		1900		1906		1905		Fe-MoO_3
1886								Fe-MoO_3
		1852	1852	1840	1851	1846	1843	Fe-MoO_3
					1800			Co-MoO_3
	1761			1780		1782	1778	Fe-MoO_3
1748						1730		Fe-MoO_3
				1715	1713			Fe-MoO_3
		1697	1695	1688		1693	1685	Co-MoO_3
				1653				Co-MoO_3
1612	1615					1620		Fe-MoO_3
			1542		1562	1550	1540	Fe-MoO_3
	1505	1511		1525		1511		Fe-MoO_3
			1499		1488			Fe-MoO_3
						1462	1450	Fe-MoO_3
1417	1406							Fe-MoO_3
		1396	1385		1388			Co-MoO_3
				1377		1369	1372	Fe-MoO_3
	1307						1306	Fe-MoO_3
		1280	1296		1271	1280		Co-CO_3
					1237			Co-CO_3
				1200				Co-CO_3
	1144						1160	Fe-MoO_3
			1113			1104		Co-CO_3
					1099			MoO_3 BP*
				1075	1077	1061		MoO_3 BP*
							1032	MoO_3 BP*
		992	989	975	982	975	972	Mo=O
967	952	947						Mo-O
				921	929	935		Mo-O
			909					Mo-O
882	887						890	Mo-O
			831	834	825		826	Mo-O
						815		Mo-O
747			753		764			Mo-O
	712				712			Fe-O

*BP=Bulk Phase

III. Effect of Method of preparation:

FTIR Studies:

Tables 16-20 present the data on the vibrational frequencies indicating the effect of method of preparation. For a given metal concentration and a particular metal loading the vibrational modes excited were analyzed to study the effect of method of preparation. The striking difference between co-precipitation samples and pyrolysis samples is that more Fe-MoO_3 or Co-MoO_3 ligand surface structures that are IR active are promoted in the latter samples. Also, it seems that pyrolysis samples are less reactive to CO and syngas exposure compared to co-precipitation samples, since many of the surface structures occurring in the pyrolysis precursors seem to persist even after exposure to CO or syngas with not many new modes emerging.

Further, reduction of co-precipitation samples leads to suppression of original vibrational modes in the precursor stage and generation of new vibrational modes. In pyrolysis samples while reduction suppresses original vibrational modes in the precursor, not many new modes are generated. Many of the precursor vibartional modes persist even after exposure to CO with generation of very few new modes in both co-precipitation and pyrolysis samples. Many of the high frequency vibrational modes present in the precursor, reduced, and CO exposed samples are suppressed due to syngas exposure in co-precipitation samples. In pyrolysis samples, however, many high frequency modes observed in precursor persist with generation of few new modes.

It is observed that the samples prepared by co-precipitation have higher reactivity towards bond breakage of the model compounds than those prepared with pyrolysis method. Otherwise, the reactivity in both series is similar.

Pyrolysis samples seems to be more amenable for reduction compared to co-precipitation samples as by the saturation magnetization and susceptibility values shown in tables 11 and 12.

TABLE 21: Effect of method of preparation: Fe-Co-MoO_3 (Fe/Co=0.3) ML=5%

Precursor		Reduced		+ CO		+(CO+H_2)		
CoPrecipation	Pyrolysis	CoPrecipation	Pyrolysis	CoPrecipation	Pyrolysis	CoPrecipation	Pyrolysis	
1950	1956		1932		1946	1940	1945	Fe-MoO_3
1922	1919	1903	1903				1908	Co-MoO_3
1880	1888							Fe-MoO_3
					1859		1844	Co-CO_3
					1802			Co-CO_3
							1776	Co-CO_3
	1732		1722		1738		1706	Fe-MoO_3
	1662				1657		1647	Co-MoO_3
1621	1598				1605			Fe-MoO_3
	1533		1558		1533	1510	1530	Fe-MoO_3
	1481			1456	1472			Fe-MoO_3
	1417				1415			Co-MoO_3
	1374	1386	1393					Co-MoO_3
					1357		1343	Fe/Co-MoO_3
							1290	Co-CO_3
					1250	1251	1228	Co-CO_3
1142	1128					1146	1156	Fe-MoO_3
		1104	1108	1101	1107	1102	1105	Fe/Co-MoO_3
	1067						1063	MoO_3 BP*
		1005	1008	1015	1024	1001	1016	MoO_3 BP*
994								Mo=O
	921	930	927	937	916	927	920	Mo-O
874					870		869	Mo-O
832	849		845					Mo-O
		799				808		Mo-O
749			762	752	758		756	Mo-O
	719							Fe-O

*BP=Bulk Phase

TABLE 22: Effect of method of preparation: Fe-Co-MoO_3 (Fe/Co=0.3) ML=15%

Precursor		Reduced		+ CO		+($CO+H_2$)		Assignments
CoPrecipation	Pyrolysis	CoPrecipation	Pyrolysis	CoPrecipation	Pyrolysis	CoPrecipation	Pyrolysis	
1923	1954		1941			1939	1947	Fe-MoO_3
	1920	1901	1905		1928		1903	Co-MoO_3
1879	1886				1866		1859	Fe-MoO_3
		1811			1808			Co-CO_3
		1724	1730		1733	1717		Fe-MoO_3
		1687			1667	1664	1680	Co-MoO_3
1615	1615				1623			Fe-MoO_3
		1583		1583	1576	1584	1573	Co-MoO_3
		1524					1504	Fe-MoO_3
		1486	1495	1486	1491	1478		Fe-MoO_3
1408	1410			1420		1450		Fe-MoO_3
		1385						Co-MoO_3
		1326			1334	1301	1342	Co-MoO_3
				1269		1268		Co-MoO_3
						1234	1208	Co-CO_3
1127	1127							Fe-MoO_3
		1102		1112		1109	1105	Fe-MoO_3
	1071			1035	1036	1060	1046	MoO_3 BP*
		1007	1009	1007		1006		MoO_3 BP*
991				978	960		951	Mo=O
963	937	940	946	932		927		Mo-O
832	863		851		889		884	Mo-O
				801		807	805	Mo-O
731			771		744		754	Mo-O
	709					681	704	Fe-O

*BP=Bulk Phase

TABLE 23: Effect of method of preparation: Fe-Co-MoO_3 (Fe/Co=1.5) ML=5%

Precursor		Reduced		+ CO		+(CO+H_2)		Assignments
CoPrecipation	Pyrolysis	CoPrecipation	Pyrolysis	CoPrecipation	Pyrolysis	CoPrecipation	Pyrolysis	
1939	1955		1942				1946	Fe-MoO_3
		1903			1927		1909	Co-MoO_3
	1885						1866	Fe-MoO_3
			1736		1713			Co-CO_3
1621								Fe-MoO_3
			1567				1568	Co-MoO_3
					1523	1520		Fe-MoO_3
			1441	1460				Co-MoO_3
					1401			Co-CO_3
						1267		Co-CO_3
							1152	Co-CO_3
1121	1129	1112	1118	1102	1116	1105	1104	Fe/Co-MoO_3
	1076						1052	MoO_3 BP*
					1026		1017	MoO_3 BP*
		1007		1008		1006		MoO_3 BP*
994	958	942	937	937	936	930	941	Mo-O
			862		863		844	Mo-O
825	819							Mo-O
					759		765	Mo-O

*BP=Bulk Phase

TABLE 24: Effect of method of preparation: Fe-Co-MoO_3 (Fe/Co=1.5) ML=15%

Precursor		Reduced		+ CO		+(CO+H_2)		Assignmen
CoPrecipation	Pyrolysis	CoPrecipation	Pyrolysis	CoPrecipation	Pyrolysis	CoPrecipation	Pyrolysis	
1936	1952					1945	1940	Fe-MoO_3
	1919	1901	1901	1910		1910		Co-MoO_3
	1883							Fe-MoO_3
		1841	1841	1856		1850	1860	Co-MoO_3
1727	1748		1748			1741	1725	Fe-MoO_3
		1705	1710		1714			Co-MoO_3
				1678		1651	1666	Co-MoO_3
1608	1608							Fe-MoO_3
			1545		1540		1557	
		1511		1515				
						1466	1483	Co-CO_3
1427		1395	1423			1430	1404	Co-MoO_3
					1376		1329	Co-CO_3
				1270			1275	Co-CO_3
							1178	Co-CO_3
1127	1129	1115		1102		1104	1109	Fe/Co-MoO_3
		1005		1005	1000	1006		MoO_3 BP*
993			998	967		971		Mo=O
	903	939				923	938	Mo-O
							863	Mo-O
820	817	822						Mo-O
			784		781			Mo-O
					706			Fe-O

*BP=Bulk Phase

TABLE 25: Effect of method of preparation: Fe-Co-MoO_3 (Fe/Co=1.5) ML=25%

Precursor		Reduced		+ CO		+(CO+H_2)		Assignment
CoPrecipation	Pyrolysis	CoPrecipation	Pyrolysis	CoPrecipation	Pyrolysis	CoPrecipation	Pyrolysis	
1938	1919						1913	Fe/Co-MoO_3
		1853	1852		1851	1850	1843	Fe-MoO_3
					1800			Co-MoO_3
1764	1761					1741	1778	Fe-MoO_3
					1713			Co-CO_3
		1675	1695	1662		1651	1685	Co-MoO_3
1612	1615							Co-MoO_3
			1542	1589	1562		1540	Fe-MoO_3
	1505	1482	1499	1461	1488	1466	1450	Fe-MoO_3
1416	1406			1415		1430		Co-MoO_3
			1385		1388		1372	Co-CO_3
	1307		1296				1306	Co-MoO_3
				1276	1271			Co-CO_3
					1237			Co-CO_3
	1144					1150	1160	Fe-MoO_3
1115			1113	1105	1099	1104		Fe/Co-MoO_3
					1077		1032	MoO_3 BP*
		1002		1005		1006		MoO_3 BP*
961	952	960	989	969	982	971	972	Mo=O
		940		931	929	923		Mo-O
895	887	895	909				890	Mo-O
			831		825		826	Mo-O
			753		764			Mo-O
	712				712			Fe-O

*BP+Bulk Phase

TABLE 26: Effect of method of preparation: Fe-Co-MoO_3 (Fe/Co=1.5) ML=5%

Precursor		Reduced		+ CO		+($CO+H_2$)		Assignments
CoPrecipation	Pyrolysis	CoPrecipation	Pyrolysis	CoPrecipation	Pyrolysis	CoPrecipation	Pyrolysis	
	1956				1946		1945	Fe-MoO_3
	1924		1932					Co-MoO_3
		1902	1903		1908		1909	Fe-MoO_3
1883	1887			1854	1864			Co-MoO_3
	1771				1791		1775	Fe-MoO_3
	1721			1740				Co-MoO_3
	1663	1683	1707		1687		1679	Co-MoO_3
1614				1624			1607	Fe-MoO_3
	1596		1548		1570		1564	Co-MoO_3
				1502			1515	Fe-MoO_3
	1476				1476		1484	Co-MoO_3
	1434				1440		1430	Co-MoO_3
1413			1392		1400	1389	1400	Co-MoO_3
				1354				Co-CO_3
					1300		1300	Co-CO_3
		1269				1273		Co-MoO_3
					1226		1228	Co-CO_3
					1153		1156	Co-CO_3
1124	1127		1107		1104	1106	1105	Fe/Co-MoO_3
	1075				1062		1061	MoO_3 BP*
				1025	1020	1039	1017	MoO_3 BP*
			1005					MoO_3 BP*
985	963	997		962	978		977	Mo=O
			936		938	942	940	Mo-O
	898		870		875		868	Mo-O
				842	853			Mo-O
	825							Mo-O
748			725		764	733	762	Mo-O
	709					693		Fe-O
		673				676		Fe-O

*BP=Bulk Phase

TABLE 27: Effect of method of preparation: Fe-Co-MoO_3 (Fe/Co=3.0) ML=15%

Precursor		Reduced		+ CO		+($CO+H_2$)		Assignments
CoPrecipation	Pyrolysis	CoPrecipation	Pyrolysis	CoPrecipation	Pyrolysis	CoPrecipation	Pyrolysis	
1942							1946	Fe-MoO_3
	1921	1903	1901		1909			Co-MoO_3
1881	1882			1864	1866	1861	1864	Fe-MoO_3
		1840	1840		1825			Co-MoO_3
							1793	Fe-MoO_3
	1749				1731	1715	1717	Co-MoO_3
		1692	1693	1693	1680			Co-MoO_3
							1652	Co-CO_3
1615	1611				1600			Fe-MoO_3
	1566		1540				1540	
	1502	1518		1512	1499	1517		Fe-MoO_3
1415	1411						1400	Co-MoO_3
		1394	1356		1388			Co-MoO_3
	1327				1325		1320	Fe-MoO_3
						1266	1264	Co-CO_3
				1232	1227		1190	Co-CO_3
					1159		1152	Co-CO_3
1119	1123							Fe/Co-MoO_3
	1030				1035		1050	MoO_3 BP*
			995	1019		1018		MoO_3 BP*
971	956	954	960	977	977			Mo=O
					938	939		Mo-O
	901		897					Mo-O
	865				843		843	Mo-O
			816					Mo-O
791	793				757	735		Mo-O
				673			708	Fe-O

*BP=Bulk Phase

TABLE 28:Effect of method of preparation: Fe-Co-MoO_3 (Fe/Co=3.0) ML=25%

Precursor		Reduced		+ CO		+(CO+H_2)		Assignment
CoPrecipation	Pyrolysis	CoPrecipation	Pyrolysis	CoPrecipation	Pyrolysis	CoPrecipation	Pyrolysis	
1924	1928							Fe-MoO_3
			1900		1906		1905	Co-MoO_3
	1886							Fe-MoO_3
		1851	1852	1858	1840	1854	1846	Co-MoO_3
					1780		1782	Fe-MoO_3
1738	1748				1715		1730	Co-MoO_3
		1695	1697	1682	1688		1693	Co-MoO_3
					1653	1645		Fe-MoO_3
1615	1612						1620	Co-MoO_3
							1550	Co-CO_3
		1515	1511	1500	1525	1521	1511	Co-CO_3
							1462	Co-CO_3
1417	1417							Co-MoO_3
		1385	1396	1384	1377		1369	Co-MoO_3
		1289	1280	1289			1280	Co-MoO_3
					1200			Co-CO_3
1148							1104	Fe/Co-MoO_3
					1075	1048	1061	MoO_3 BP*
			992					Mo=O
	967	968	947	968	975	977	975	Mo-O
					921		935	Mo-O
896	882							Mo-O
					834	826	815	Mo-O
	747							Mo-O
						691		Fe-O

*BP=Bulk Phase

SUMMARY

1. FTIR spectra of Fe-MoO_3 catalysts indicate that, exposure to syngas dissociate MoO_3 structures with iron but inhibit generating carbonyls of iron. In these catalysts iron carbides might be forming instead of carbonyls which are necessary intermediate products for the formation of longer chain hydrocarbons. Even though iron with other supports is known to be a hydrocarbon selective catalyst, with MoO_3 as support, it seems to be a poor syngas conversion catalyst.

- The catalytic data obtained through indirect liquefaction shows a drop in higher hydrocarbon production, the product being mostly methane.

- Direct liquefaction results show no bond cleavage supporting FTIR and indirect liquefaction findings.

- Magnetization data support these findings indicating the presence of Fe^{2+} ions in CO and $CO+H_2$ exposed catalysts.

- Method of preparation seems to have no significant influence on the observed results.

- In Fe/Co/MoO_3 catalysts, exposure syngas seems to replace MoO3 with CO and probably generating cobalt carbonyls structures.

- Magnetization studies indicate that exposure to CO and syngas seems to enhance reduction to metalic state promoting dissociation of MoO_3 from Fe/Co/MoO_3 complex

- Direct liquefaction studies support these findings, indicating bond cleavage NBBM. The major product being naphthalene, methyl bi-benzyl, methyl naphthalene.

- Method of preparation nor inter-metallic ratio does not seem to produce significant changes in the observed results

- The results suggest Fe-Co-MoO_3 might be a suitable candidate for syngas conversion compared to Fe-MoO_3 catalysts

REFRENCES

1. Derbyshire F.J. Energy and Fuels 3, 273 (1989)

2. Hancock, K.G., Ed., Chemistry Newsletter, *NSF announces a New Program for Materials Synthesis and Processing(MS&P)*, page 1, August (1991) issue

3. Kinkade N.E., (Union Carbide Corporation) EP-0149255 (1985).

4. Xu Xiaoding, I.B.M. doesburh and J.J.F. Scholten. Catalysis Today, 2, 125 (1987)

5. Bommannavar A.S., and Montano P.A. Fuel 61, 523 (1982); and Montano P. A., and Granoff B. Fuel 59, 214 (1980)

6. Gossard, A.C., and A.M. Portis, Suppl. J. Appl. Phys., 31, 205 (1960).

7. Selwood, P.W. "Magneto Chemistry", Inter. Sci. Publishers. (1956), "Chemisorption and Magnetization", Academic Press, New York (1975).

8. Wohlforth, E. P., "Ferromagnetic Materials", North Holland (1980) and D.J. Craik, "Magnetic Oxides", Wiley, New York (1975).

9. Bean, C.P., and J.D. Livingston, J.Appl. Phys., 30, 1205 (1959).

10. Luborsky, F.E., J. Appl. Phys. 33, 1909 (1959).

11. Candela, G.A., R.A. Haines Appl. Phys. Lelt. 34, 868 (1979).

12. Kneller Eckart "Fine Particle Theory - in Magnetism and Metallurgy" (Editor) Ami. Berkowitz, Academic Press 365-471.

13. Murty, A.N., A.A. Williams, R.T. Obermyer, and V.U.S. Rao, J. Appl. Phys., 61, 4361 (1987).

14. Murty, A.N., A.A. Williams, R.T. Obermyer, V.U.S. Uao, and R.J. Gomley. Surface Science and Catalysis (1987) (Ed. J.W. Ward) PP 73-80, Elsevier Science Publishers, B.V. Amsterdam (1988).

15. Murty, A.N., M. Seamster, A.N. Thorpe, R.T. Obermyer, V.U.S. Rao. J. Appl.

Phys. 67, 5847, (1990).

1 6 Murty, A.N. "New Method of Magnetic Characterization of Zeolite Cobalt Catalysts"Final
Technical Report U.S. D.O.E. Grant DE-FG22-85PC 80536,Aug 31, (1988).

17. Murty, A.N. "NMR Investigation of Supported Metal Catalysts for Syngas Conversion" Final Technical Report. U.S. DO.E. Grant DE-FG22-87PC-79917. Nov 1, 1990

18. Murty, A.N., Donatto, U.A., Washington, J.W. Hoard, T.L., Akundi, M.A., and Harris, C., IEEE Transactions on Magnetics, 30, 4722, 1994

19. Murty, A.N., "NMR – NQR studies of Higher Alcohol Synthesis Cu-Co Catalysts", Final Technical Report U.S. D.O.E. Grant DE-FG22-89PC8976 (M003), March 1995.

20. Zafiris, G.S., and R.J. Gorte, J. Cat. 132, 275, (1991).

21. Decanio, E.C., and D.A. Storm, J. Cat. 132, 275, 1991.

22. Yan Y., Q. Xin, S. Jiang and X. Guo, J. Cat., 131, 234, (1991).

23 Balliard-Letrournel, R.M., Gomez Cobo, A.J., Mirodotos, C., Primet, M., and Dalmon, J.A., caatalysis Letters, 2,149,(1989).

24. Mouaddib, N., Perrichon, V., and Primet, M., J. Chem. Soc.Farad. Trans. 85, 3413,

(1989); Proc.9th. Int. Congr. Catal. 2, 521,(1988).

25. Akundi, M.A., Rao, D.V.K., and Rao, P.T., Proc. Roy. Ir. Academy, A73, 212, (1973)

26. Akundi, M.A., Putcha, V., and Basu S.K., Ind.J.Phys 53B, 388, (1980)

27. Byung, KNA, Walters, BA, and Vannice, M.A., J.Catal, 140, 585(1993).

28. Hamedh, M.I, and King D ., J. catal, 88, 264(1972).

29. Venter, J.J and Vannice, M.A ., Appl. Spectrosc, 42, 1096 (1988).

30. Venter J.J and Vannice, M.A., J. Am.Chem.Soc III, 2377(1989)

32. Augustine S.M, and Blitz, J.P., J. Catal, 142, 312(1993).

25. Bauer, J., Brian, B.W., Butter, S.A., Dyer, P.N., Parsons, R.L., and Pierantozzi, "*Catalytic Conversion of Synthesis Gas and Alcohols to Chemicals,*" Herman, R.G., Ed., Plenum Pree,p-129 (1984).

33. Hall, C.C., Gall, D., and Smith, S.L., J. Inst. Pet., 38,845 (1952).

34. Farlet, R., and Ray, D.J., J. Inst. Pet ,50, 27 (1964).

35. Satterfield, C.N., and Huff, G.A., J. Catal., 73, 187 (1982); 85, 370 (1984).

36. Schneider M. K. Kochloefl O. Bock. (Sud Chemie) EP-0152809- A2 (1985).

37. Ichikawa M. Bull. Chem. Soc. Japan 51, 2268, 2273 (1978).

38. Kinkade N.E. (Union Carbide Corporation) EP-0149255 (1985).

39. Quardere G.J. G.A. Cochran (DOW Chemical) EP-0119609-Al (1984).

40. Institute Francois Du Petrole. UK Patents: GB 2118061A(1983), GB 2158730A (1985), U.S. Patent 4,291,126 (1981).

41. Xu Xiaoding, I.B.M. doesburh and J.J.F. Scholten. Catalysis Today, 2, 125 (1987).

.

42. Ichikawa M., Bull. Chem. Soc. Japan, 51, 2268, 2273 (1978).

43 Lee, J-F, Chern, W-S, Lee, M-D, Can., J. Chem., 70,511 (1992).

44 Teichner S. J. Proc. 1st Aerogel Symposium, 22 (1986).

45. Kistler S.S. J.Phys. Chem. 36, 52 (1932).

46. Marcilly C., P. Courty, and B. Delmon. J. Am. Cer. Soc., 53, 56 (1970).

47. Blanchard F., J.P. Reymond., B. Pommier, and S. J. Teichner J. Mol.Catal, 17, 171 (1982).

48. B. Pommier., J. P. Reymond., and S. J. Teichner "*Catalysis on the energy Scene*", S. Kaliaguine and A. Mahay Eds. Elesevier, Amsterdam, p.471 (1984).

49. Belhekar, A.A., Ayyappan, S., Ramaswamy, A.V., J. Chem.Tech.Biotechnol., 59,395, (1994)

50. M.R. Sun-Kou, A. Mendioroz, J.L.G. Fierro, and J.M. Palacios, *Journal of Materials Science*, 30, p. 496, 1995.

51. A.A. Davydov, "Infrared Spectroscopy of adsorbed species on the surface of transition metal oxides," John Wiley and sons, (1990)

52. Danon , J. In Chemical applications of Mossbauer Spectroscopy, Goldanski, V.I., Ed., Herber, R.H., Academic Press, P212 (1968)

53. Walker, L.R., Werthiem, G.K., Jaccarino, V., Phys. Rev. Lett., 6,98,(1961)

54. Final report # DE-FG-22-93MT93010, April (1998)

55. F.V. Stohl, and K.V. Diegert, Energy & Fuels 8,117-123.1994,

ACKNOWLEDGEMENTS

The investigators would like to thank the Department of Energy for providing the financial support for this project. We sincerely thank Dr. F.J. Waller, Air Products Inc., for conducting the catalytic studies on Fe/moo3 catalysts. His valuable support and guidance is greatly appreciated. We would like to extend our thanks to Dr. Udaya S. Rao, the technical project Officer, for his valuable guidance and support through out the project period. One of the investigators would like to thank Ms. Adrienne Hunter for her valuable time in typing the report.

Minority Undergraduate Student Training: Papers Presented

"Magneto-Chemical character studies on FE-Mo catalysts" Akundi, M., D.Washington*, ,J.Zhang, , and A.N.Murty, Grambling state University,71st Louisiana Academy of Science meeting , Momroe, Louisiana ,February, 1997.

"FTIR studies of syngas interactions on Fe-Co-MoO_3 composite catalyst" Gibbs.M*, D. Washington*, and M.A. Akundi, Xavier University of Louisiana. 73rd Louisiana Academy of Science meeting,February 1999

"Catalytic Character analysis of Fe-Mo system by Mossbauer and FTIR spectroscopy techniques" M. Gibbs*, S.Davis*, M.Akundi, J.Zhang, N.Seetala, and Murty A.N. Proceedings of the National Conference on Undergraduate Research, Vol V, 1416, 1999

"Magneto – Chemical characterization of Fe/Co syngas conversion catalysts"
E. Bruster*, L. Turner*, T.Porter*, S.Davis*, M.A.Akundi, S.V.Naidu, and A.N.Murty
Proceedings of the 'Material Science in the State of Louisiana Conference' University of New orleans, New Orleans, August 17-18, 2000, Louisiana

FTIR and Magnetization studies of syngas interaction withFe/MoO_3 and $Fe/Co/MoO_3$ Catalyst", Monique L. Gibbs*, Misty M. Watson*, E. Bruster*, L.Turner*, Murty A. Akundi and A.N.Murty, Proceedings of the National Conference on Undergraduate Research, Rochester, 2000

"Effect of method of preparation on the FTIR and Magnetic character of Coal Liquefaction Catalysts" Akundi, M.A., Zhang, J., Gibbs, M*, Laury, N*., and Watson, M*., Murty, A.N., 74th Louisiana Academy of sciences meeting, Shreveport, La, February, 2000

"Molyybdenum oxide supported liquefaction Catalysts: synthesis characterization,and model compound reactivity" Nina ray*, M.A. Akundi, J.Zhang, Louisiana Stokes Alliance for Minority participation Research Conference, New Orleans, September, 2000

"Reactivity of Iron, Cobalt and Molybdenum based catalysts for Model compound of Coal Liquefaction", Nina ray*, M.A. Akundi, J.Zhang Presented at undergraduate research poster session of Joint southeast Regional ACS meeting, New Orleans, December, 2000,

Magneto-chemical character studies of Iron - Moly and Iron - Cobalt-Moly catalysts" M.A.Akundi, J.Zhang, M. Gibbs*, M.M.Watson*, E.Bbruster* L.Turner*. A. N Murty, N.Seetala, and F.J.Waller, IEEE Transactions on Magnetics, 37, 2929, 2001

"Syngas Interactions on Iron – Moly and Iron-Cobalt – Moly catalysts: Effect of Method of Preparation" J.Muslim*, M.Wartson*, M.A.Akundi, J.Zhang, Proceedings of the National Conference on Undergraduate Research, Lexington, 2001

* Minority undergraduates participated in the project